

Series Resistance Increase in Field Degraded PV Modules in
Different Climatic Conditions

by

Viswa Sai Pavan Buddha

A Thesis Presented in Partial Fulfillment
of the Requirements for the Degree
Master of Science

Approved November 2018 by the
Graduate Supervisory Committee:

Govindasamy Tamizhmani, Chair
Terry Alford
Devarajan Srinivasan

ARIZONA STATE UNIVERSITY

DECEMBER 2018

ABSTRACT

Global photovoltaic (PV) module installation in 2018 is estimated to exceed 100 GW, and crystalline Si (c-Si) solar cell-based modules have a share more than 90% of the global PV market. To reduce the social cost of PV electricity, further developments in reliability of solar panels are expected. These will lead to realize longer module lifetime and reduced levelized cost of energy. As many as 86 failure modes are observed in PV modules [1] and series resistance increase is one of the major durability issues of all. Series resistance constitutes emitter sheet resistance, metal-semiconductor contact resistance, and resistance across the metal-solder ribbon. Solder bond degradation at the cell interconnect is one of the primary causes for increase in series resistance, which is also considered to be an invisible defect [1]. Combination of intermetallic compounds (IMC) formation during soldering and their growth due to solid state diffusion over its lifetime result in formation of weak interfaces between the solar cell and the interconnect. Thermal cycling under regular operating conditions induce thermo-mechanical fatigue over these weak interfaces resulting in contact reduction or loss. Contact reduction or loss leads to increase in series resistance which further manifests into power and fill factor loss. The degree of intermixing of metallic interfaces and contact loss depends on climatic conditions as temperature and humidity (moisture ingress into the PV module laminate) play a vital role in reaction kinetics of these layers. Modules from Arizona and Florida served as a good sample set to analyze the effects of hot and humid climatic conditions respectively. The results obtained in the current thesis quantifies the thickness of IMC formation from SEM-EDS profiles, where similar modules obtained from different climatic conditions were compared. The results indicate the thickness of the IMC and detachment degree to be growing with age and operating temperatures of the module. This can be seen in Cu_xSn_y IMC which is thicker in the case of Arizona module. The results obtained from FL

aged modules also show that humidity accelerates the formation of IMC as they showed thicker Ag_xSn_y layer and weak interconnect-contact interfaces as compared to Arizona modules. It is also shown that climatic conditions have different effects on rate at which Cu_xSn_y and Ag_xSn_y intermetallic compounds are formed.

ACKNOWLEDGMENTS

First, I would like to thank my professor Dr. Govindasamy Tamizhmani for giving me this wonderful opportunity to work under him at Photovoltaic Reliability Laboratory. His continuous support, constant encouragement and his valuable inputs to my work irrespective of his busy schedule have been invaluable to my work and me. I would like to thank Dr. Terry Alford and Dr. Devarajan Srinivasan for serving on my thesis committee and for their valuable inputs. I would also like to thank Dr. Archana Sinha of Photovoltaic reliability Laboratory for her valuable inputs throughout my thesis and constantly clarifying my queries whenever requested. Some of the results presented in this thesis are based on the modules provided by FSEC (Dr. Kristopher Davis, Dr. Eric Schneller). The kind support of FSEC is gratefully acknowledged. I acknowledge the use of facilities within the Eyring Materials Center at Arizona State University supported in part by NNCI-ECCS-1542160. I would also like to thank my colleagues who worked with me especially Mr. Sai Tatapudi, our technical manager, Hamsini, Aesha Patel, Prathamesh Thorat and Shreyas Whagmare for helping me out with my experiments whenever I requested help. Finally, I would like to thank the lord almighty for making all this happen.

Thank you all. Thanks a ton.

To,

My beloved parents, Kameswara Rao Buddha and Kiranmayi Buddha, my sister Harshitha and all other family members and friends who made me what I am with their constant support and encouragement.

TABLE OF CONTENTS

	Page
LIST OF TABLES	vii
LIST OF FIGURES	viii
1.Introduction.....	1
1.1 Background	1
1.2 Statement of the problem	2
1.3 Objective	3
2 Literature review	4
2.1 Series resistance of PV device	4
2.2 Contribution of Solder bond degradation to series resistance.....	5
2.3 IMC formation and its effects	5
2.4 Effect of Moisture and temperature on IMC formation	6
3. METHODOLOGY	8
3.1 Sample selection.....	9
3.2 IV Characterization	11
3.3 EL imaging.....	12
3.4 IR imaging.....	13
3.5 Cell cutting and cell level IV	14
3.6 SEM imaging	16
3.7 Sample preparation for SEM and EDS analysis	16
3.8 EDS analysis	20
4. Experimental Results	21
4.1 Module level performance evaluation.....	21

4.2 Identification of regions with degraded solder bonds	24
4.3 Imaging of degraded solder interconnects	26
4.4 Measurement of Cell level IV parameters	29
4.5 High resolution microscopy and elemental analysis	31
5. Conclusions	47
References	49

LIST OF TABLES

Table	Page
1 Specifications of different modules used for testing.....	9
2 IV performance parameters of fresh and field aged modules	23
3 Summary of results showing correlation between interconnect detachment in SEM images and cell series resistance values.....	45

LIST OF FIGURES

Figure	Page
1 (a) Cross-section view of the c-Si solar cell (b) Schematic diagram depicting various regions at the interconnect-metal contact interface.	2
2 IV curve showing increase in slope near V_{oc} for cell with R_s when compared to ideal solar cell with no series resistance.....	4
3 (a) IMC thickness growth with respect to thermal cycling (b) IMC thickness growth with respect to isothermal ageing.....	6
4 Sample set and thesis flow describing characterization techniques.....	9
5. Outdoor IV setup with two axis tracker and PV module connected in forward bias to the curve tracer for measuring IV curves.	12
6. EL imaging setup in a dark room with camera facing the PV module.	13
7 (a) Module with their cells cut and soldered for cell level DIV and LIV measurements (b) Nomenclature used to name the cells in the PV (c) solar simulator setup module.....	15
8 (a) Cutting solar cell from the module using power tool (b) Solar cell cut from the module (c) Sample cut along the interconnect region of the cell (d) Holder base coated with high vacuum grease (e) Holder cup used to contain the epoxy mix (f) Placement of the samples with the area of interest facing the base (g) Vacuum chamber used to vacuum epoxy mix (h) Uncured epoxy mix poured into the cup with samples (i) Retrieving Cured sample post 24 hours.	17

Figure	Page
9 (a) Silicon carbide grinding paper with continuous water supply (b) Polishing cured sample to get a smooth surface for SEM and EDS analysis	18
10 Optical microscope setup.....	18
11 Carbon coating setup used to coat samples with thin carbon layer	19
12 Sample placed inside the SEM holder post calibration.	20
13 (a) IV curves of fresh and field aged type-I modules (b) IV curves of fresh and field aged type-II modules	22
14 Plot depicting the degradation of IV parameters in test modules.	24
15 EL images of type-I fresh module, type-II FL aged module, type-II AZ aged module, type-II fresh module and type-II AZ aged modules in the following order.	26
16 IR images of type-I fresh module, type-II FL aged module, type-II AZ aged module, type-II fresh module and type-II AZ aged modules in the following order with red being the hottest and blue being the coldest regions.....	28
17. Maximum power (P_{max}) and Fill Factor (FF) correlation plots with series resistance (R_s) of (a) type-I fresh module (b) type-II FL aged module (c) type-II AZ aged module (d) type-II fresh module (e) type-II AZ aged modules.....	31
18 Cross-sectional SEM (top) and optical images (bottom) at 71X magnification of type-I fresh module with good interconnect along the back and front contacts of the cell.....	32

Figure	Page
19 Elemental spectral map highlighting all the elements that are present along the interconnect region.	33
20 Line scan across the interconnect region indicating the intermixing of the adjacent metallic layers.	34
21 Cross-sectional SEM and optical images of type-I FL aged high resistance cell indicating detachment of interconnects (red box) and lead segregation (blue box)	35
22 Line scan across the interconnect region of type-I FL aged sample-2, indicating voids at the cell-contact interface (highlighted by dotted lines).	36
23 Cross-sectional SEM and optical images of type-I FL aged medium resistance cell samples indicating comparatively low detachment of the interconnects.....	37
24 Cross-sectional SEM and optical images of type-I FL aged low resistance cell indicating very low interconnect detachment	38
25 Cross-sectional SEM and optical images of type-I AZ aged high resistance cell indicating severe detachment of interconnects (highlighted in red).	39
26 Cross-sectional SEM and optical images of type-I AZ aged medium resistance cell indicating comparatively low detachment	40
27 Cross-sectional SEM and optical images of type-I AZ aged low resistance cell indicating low detachment of interconnects.	40

Figure	Page
28 Cross-sectional SEM and optical images of type-II fresh module.	41
29 Line scan across the interconnect region of type-II AZ aged sample-1	42
30 Cross-sectional SEM of type-II AZ aged low resistance cell indicating low detachment of interconnects.	43
31 Line scan across the interconnect region of type-II AZ aged sample-2	43
32 Series resistance and IMC thickness boxplot of aged and fresh modules.	44

1.Introduction

1.1 Background

Photovoltaics (PV) offers the possibility to convert unlimited energy from sun into electrical energy to satisfy world-wide energy demand. According to International Energy Agency (IEA), solar energy accounted for the second highest rate of growth of all the renewable energy sources in the world. Reliability of photovoltaic modules has huge impact on their growth due to its high upfront cost. This makes it important to understand and improve the long-term degradation in PV modules. PV modules are designed to survive 25 to 30 years of outdoor operation, and improving their lifetime vastly decreases the levelized costs of electricity (LCOE) of PV systems [2]. The PV module construction can be seen in Figure 1(a). It consists of a solar cell that is sandwiched between two encapsulant layers which help bond the cell to the superstrate (glass) and the substrate (backsheet/glass) layers.

Two major degradation parameters in PV modules are short circuit current (I_{sc}) loss due to browning of encapsulant layer and fill factor (FF) loss or series resistance increase due to solder bond degradation at the cell contact and solder interconnect interface. The cell contact and solder interconnect layers can be seen in Figure 1(b).

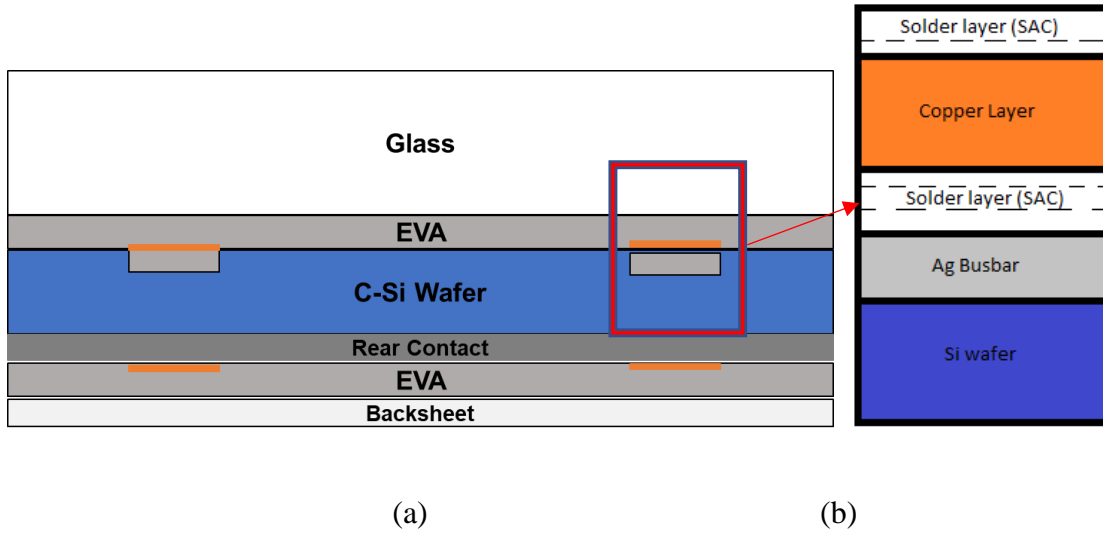


Figure 1 (a) Cross-section view of the c-Si solar cell (b) Schematic diagram depicting various regions at the interconnect-metal contact interface.

Against this background, understanding series resistance increase in solder interconnects is of importance. Temperature, humidity and other climatic conditions play a vital role in PV reliability and durability. Hence, understanding their failure mechanisms under different climatic conditions can help improving the PV module reliability and durability.

1.2 Statement of the problem

Series resistance of solar cell has multiple components, which include sheet resistance of the semiconductor, contact resistance along the semiconductor and metallic contact interface and resistance along the metallic contact and solder ribbon interface. Resistance along the metallic contact and solder ribbon primarily increases due to combination of brittle intermetallic compounds formation and contact loss. These compounds are susceptible to thermo-mechanical fatigue which results in detachment of interconnects due to coefficient of thermal expansion (CTE)

mismatch among different adjacent layers. The formation of cracks and voids leading to contact loss at interconnect interface will result in power loss which will eventually affect the levelized cost of energy (LCOE). The mechanism of IMC formation is fairly understood in the electronic and PV industry but it's important to validate their results under field conditions as there could be multiple factors that effects IMC formation. Hence, it is important to understand and quantify the effects of temperature and climatic conditions on intermetallic compounds (IMC) formation and detachment of interconnects.

Correlating the IMC thickness and detachment of interconnects with the performance parameters of the field aged PV modules will help understanding the effects of climate on the reliability of PV modules.

1.3 Objective

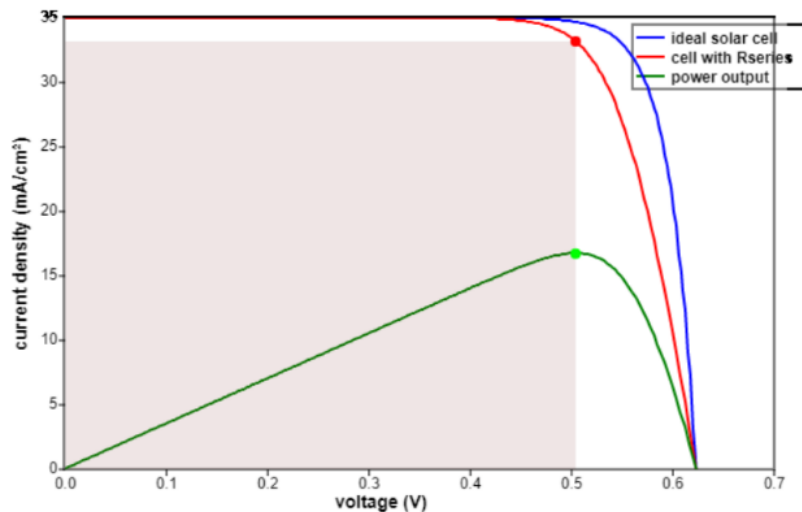
The objective of the thesis is to understand the cause and effects of series resistance increase in field degraded PV modules installed in different climatic conditions. This includes identification of degraded mechanisms in field aged modules from different climatic conditions and establishing the correlation between the series resistance, solder bond degradation and performance loss by comparing SEM, EDS and current-voltage (I-V) characteristics.

Estimation of IMC thickness. Effect of climate and solder bond type on solder bond degradation and R_s increase

2 Literature review

2.1 Series resistance of PV device

The PV module contacts must collect the electrons generated in the solar cell and conduct it with least resistance losses to be efficient. Pysch et al. revealed that an increase of $1 \Omega\text{cm}^2$ in series resistance reduces the fill factor by $\sim 5\%$ absolute [3]. Series resistance effects the performance of the cell by reducing the fill factor and P_{max} of the solar cell [4]. This emphasizes the fact that the components of series resistance i.e. contact resistance and solder bond resistance needs to be kept low for efficient solar cell operation.



Cell series resistance, $R_S = 1.31 \Omega \text{ cm}^2$

Figure 2 IV curve showing increase in slope near V_{oc} for cell with R_S when compared to ideal solar cell with no series resistance.

2.2 Contribution of Solder bond degradation to series resistance

Solder bond degradation is formation of brittle intermetallic compounds followed by contact loss due to thermo mechanical fatigue. Uich et al. reported two types of crack at the solder joint interfaces [5]. C. The crack at the interface between Cu ribbon and Ag electrode may be due to Ag leaching. The crack inside solder joint composed of large grain growing by repeated thermal stress is typical long-term fatigue. This phenomenon leads to contact losses which manifests into performance losses. Quantifying the extent to which solder bond degradation and contact loss effects the series resistance is largely unclear [6]. This work here tries to show the correlation between the formation of IMC and contact loss with the degradation observed in field aged modules.

2.3 IMC formation and its effects

During soldering, some of the metal substrate is dissolved into the molten solder. As a result, the solder becomes supersaturated with the dissolved metal and a thin layer of an intermetallic compound is formed at the metal–solder interface [7]. The intermetallic layer continues to grow after solidification while in field due to thermally activated solid state diffusion mechanisms. The phase growth of IMC under isothermal ageing and over number of cycles during thermal cycling is shown in Figure 3. The comparison here shows that the thickness of IMC in the case of isothermal ageing is higher than the thermal cycling due to the limited amount of time that the solder bond is at elevated temperatures. This difference in IMC formation makes it important to evaluate the rate at which IMC grows in realistic outdoor conditions.

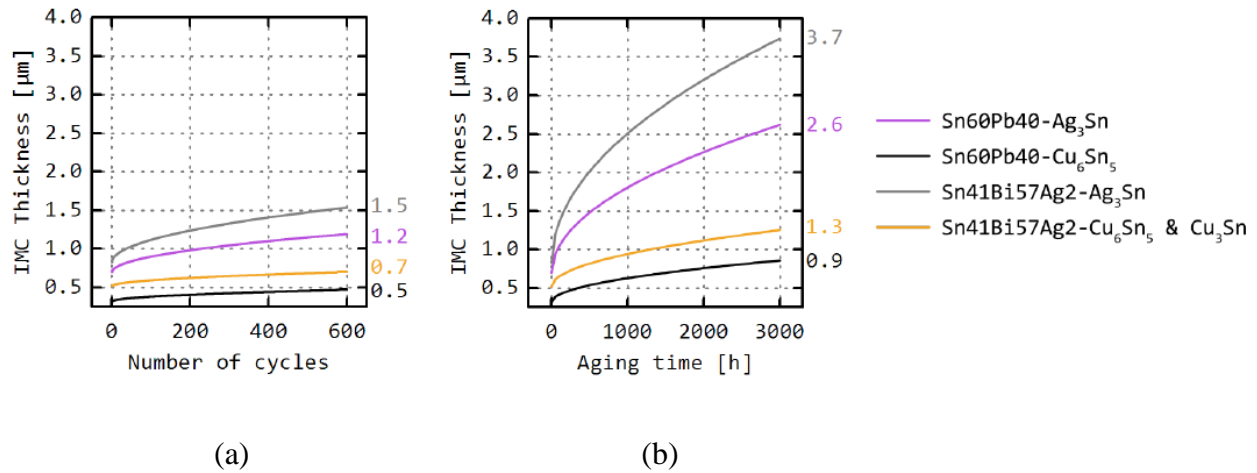


Figure 3 (a) IMC thickness growth with respect to thermal cycling (b) IMC thickness growth with respect to isothermal ageing.

The formation and growth of intermetallic at the solder/substrate interface affect the reliability of electronic joints [8]. The existence and growth of IMC within solder bonds influences the lifetime of the interconnections [6] as the solder joints turn brittle and are more susceptible to temperature cycles and humidity in the field.

2.4 Effect of Moisture and temperature on IMC formation

IMC can grow due to solid state diffusion at room temperature or at elevated temperatures while in operation. As IMC layers are brittle compared to the fresh solder, they are more susceptible to fatigue. Thermal cycling due to CTE mismatch aggravates the process of crack formation and propagation [9]–[13]. This leads to void formation at the solder, contact interface which will eventually lead to detachment.

Generally, when moisture begins to penetrate the polymer and reaches the solar cell, it can weaken the interfacial adhesive bonds, resulting in delamination [14] and increased numbers of ingress paths, loss of passivation [15], and corrosion of solder joints [16], [17]. Of these possibilities, the occurrence of corrosion has one of the highest frequencies in outdoor-exposed PV modules [18]. Significant losses in PV module performance are caused by the corrosion of the cell, that is, the SiNx antireflection coating, or the corrosion of metallic materials, that is, solder bonds and Ag fingers [19], [20]. This implies that both temperature and humidity effect the growth of IMC formation. It is also shown that combination of humidity and temperature leads to higher void formation at interconnects due to oxidation of Cu substrate [21]. The effects of high temperature in dry conditions can be evaluated from AZ aged modules while effect of moderate temperature and high humidity will be compared from FL aged modules.

3. METHODOLOGY

The sample set and the process flow of the study can be seen in Figure 4. Two types of modules namely type-I and type-II were selected which are classified based on the use of solder interconnect type. Type-I having Sn-(60%) Pb-(40%) solder and Type-II having Sn-(63%) Pb-(34%) Ag-(3%) solder. The solder compositions are reported by the module manufacturers. Both the modules have the Glass/EVA/c-Si cell/EVA/backsheet construction. Type-I modules are the modules from two different climate locations, one module is Florida (FL) aged and the other one is Arizona (AZ) aged module. Arizona has a hot and dry climate which would typically have high module operating temperatures. Florida has a hot and humid climate with high moisture content in the air and moderate temperatures. Type-I AZ aged modules are 18 years old and will test the effects of temperature cycling on degradation whereas type-I FL module is 10 years old module which will test the effect of moisture ingress and moderate temperature on degradation. Type-II modules are 21 years old AZ field aged module. The modules went through IV curve tracing, Electro luminescence (EL) imaging, Infra-red (IR) imaging and cell level performance testing followed by SEM and EDS destructive analysis.

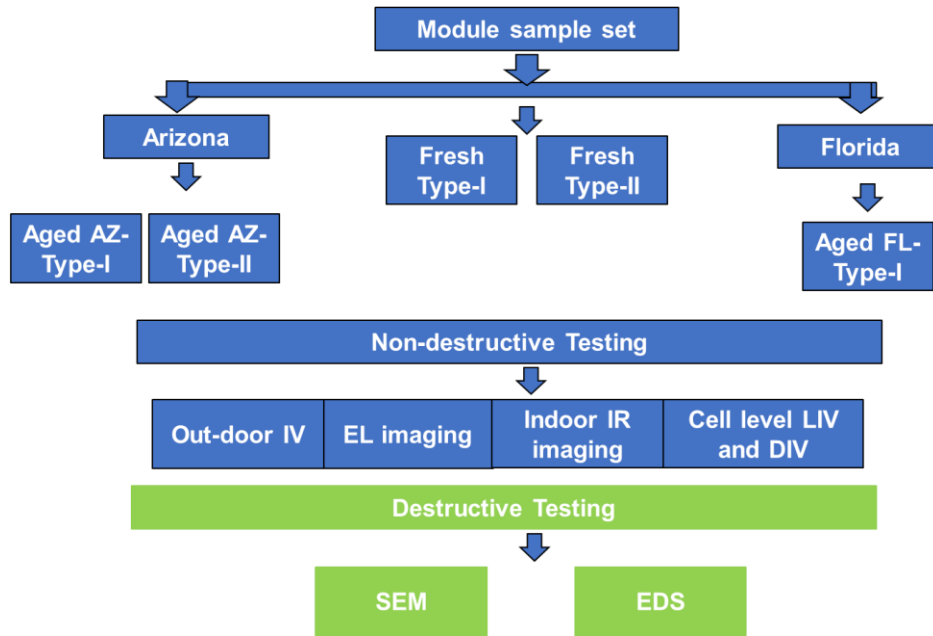


Figure 4 Sample set and thesis flow describing characterization techniques.

3.1 Sample selection

To identify effect of climate and ageing on the solder bond degradation in field degraded modules two types of aged and fresh modules from different climatic locations were selected. Table 1 shows the module specifications.

Table 1 Specifications of different modules used for testing

S.no	Module name	Cell technology	Solder type	Field exposure	Age in field (years)
1	Type I module	Mono crystalline Si	Sn-60 Pb-40	Florida exposed	10

2		Mono crystalline Si	Sn-60 Pb-40	Arizona exposed	18
3		Mono crystalline Si	Sn-60 Pb-40	Unexposed	0
4	Type II module	Poly Crystalline Si	Sn (63%)-Pb (34%)-Ag (3%)	Arizona exposed	21
5		Poly Crystalline Si	Sn (63%)-Pb (34%)-Ag (3%)	Unexposed	0

Fresh modules are not defined by any climate as they were indoors, which will be used as a reference for doing comparative studies on field aged modules. All the modules went through non-destructive module level performance testing like IV curve tracing, Electroluminescence imaging (EL), Infrared imaging (IR) followed by backsheet cutting and soldering for cell level IV measurements.

The modules were then evaluated for defects and performance degradation to select cells for interfacial SEM and EDS analysis.

3.2 IV Characterization

IV characterization is done to evaluate the health of the PV module. Daystar outdoor IV curve tracer was used under a clear sunny day with irradiance of $1000\text{W}/\text{m}^2$ and moderate wind speed. The module was placed on a two-axis tracker with the IV tracer connected in series to the module as in Figure 5. A temperature sensor (thermocouple) was connected at the center of the module backsheet to monitor the temperature during the readings. A reference cell was also mounted at the same plane of the module to measure the irradiance. A thermocouple left out open under shade was used to measure the ambient temperature. A solar dial was used to manually set the module plane perpendicular to the sunlight. The measured readings were then translated to STC conditions using a PRL excel template sheet.



Figure 5. Outdoor IV setup with two axis tracker and PV module connected in forward bias to the curve tracer for measuring IV curves.

3.3 EL imaging

EL imaging is done to detect the defects and cracks in the solar cells. It can be used to look at the intensity of luminescence emitting from the solar cell, which indicates the state of the interconnects. Solar cells generally convert photons from sunlight into electrical energy but if electrical energy is pumped in, the semiconductor emits electromagnetic (EM) waves at 1100nm wavelength as the electron jump from valence band to conduction band. These electromagnetic waves are not in the visible spectrum and a special Sensovation HR-830 pro camera is used to

detect these 1100 nm waves. The module was mounted using clamps against the wall and the camera is then placed along the line of vision to get the full images as in Figure 6. The current equivalent to I_{sc} was injected into the module under forward bias using a power supply. The exposure time was 60 seconds.



Figure 6. EL imaging setup in a dark room with camera facing the PV module.

3.4 IR imaging

IR imaging is done to identify hotspot which correspond to degraded regions along the busbar interconnects. They will consolidate the findings from EL images as, the degraded solder bonds can be detected from the hotspots in the IR image. Infrared imaging was done using Fluke Tir2 Ft thermal imager camera with a similar setup as in EL imaging. Initially I_{sc} current is injected into the module and left for 5 minutes for temperature stabilization. Images are then taken to capture defects and hotspots.

3.5 Cell cutting and cell level IV

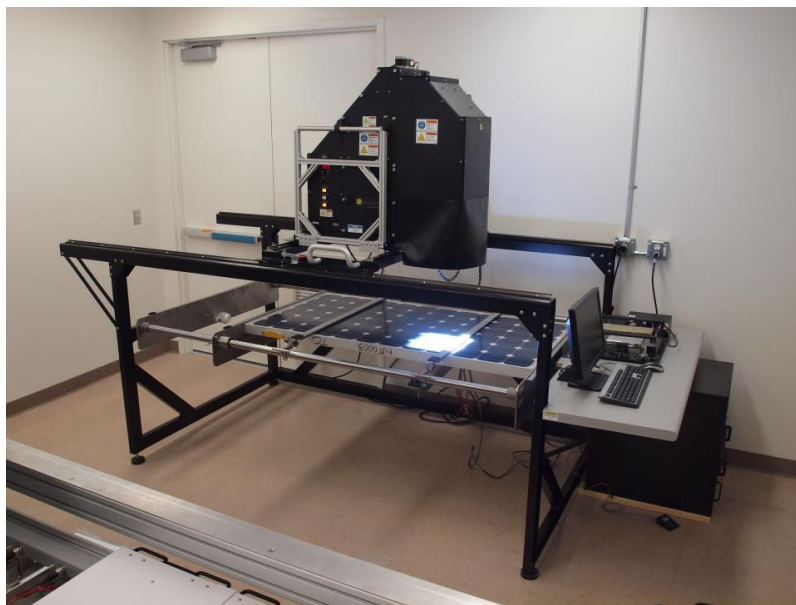
Cell level IV provides with valuable information about the series resistance of the individual cells in the module which can be used to select the cells that needs to be analyzed for IMC formation and detachment. The backsheet of all the cells were cut using a scalpel at the cell edges along the interconnect. The interconnects were then soldered with a standard tabbing ribbon using a soldering rod in the presence of a water-soluble H-20 paste flux. The soldered regions were then sealed using a Si sealant to prevent moisture and other contaminants from entering. The cut modules as in the Figure 7(a) were measured for cell level dark and light IV measurements. The cells of the module were then named as in Figure 7(b). The module was then mounted on the solar simulator for cell level IV measurements as in Figure 7(c). The temperature of the room was controlled and was set at 25°C. Each cell in the module was then connected to positive and negative probes followed by flashing the simulator lamp for IV measurements. The dark R_s values were then extracted by covering the cell with a black sheet and pumping the I_{sc} current into the cell. These results were then extracted and analyzed.



(a)

A1	A2	A3	.	.	.		
B1						Junction box	
.							
.							

(b)



(c)

*Figure 7 (a) Module with their cells cut and soldered for cell level DIV and LIV measurements
 (b) Nomenclature used to name the cells in the PV (c) solar simulator setup module*

3.6 SEM imaging

SEM imaging will help detect the defects and IMC formed at the busbar and solder bond interfaces. SEM imaging needs the sample surface to be well polished and the following section describes the sample preparation method.

3.7 Sample preparation for SEM and EDS analysis

The cells that are of interest were then cut using power tool as in Figure 8(a) and Figure 8(b). The cells were further cut into 1×1.5cm pieces as in the Figure 8(c) using high speed precision cutting tool. Silicon based high vacuum grease was then applied on the holder surface and holder cup as in Figure 8(d) and Figure 8(e) which would help remove the samples after they solidify. The samples are then placed on the reusable sample cup such that the side to be polished faces down as in Figure 8(f). The mix is then stir using a wooden stick until all the cloudy swirls disappear. The mix is then put in a vacuum chamber for 3 mins at ~28 in Hg as in Figure 8(g) to remove air bubbles which could later form pores in the cured sample.

These cut samples were then casted into cylindrical capsules using epoxy set resin and hardener as in figure. Each capsule has 3 samples from a single cell. The epoxy set process starts by weighing epoxy and hardener on a scale and mixing them in 100:12 ratio such that the mixing cup is limited to 30 grams: 3.6 grams. The mix is then casted into the sample holder as in Figure 8(h) and left overnight for the epoxy set resin to cure. The cured samples were then recovered as in Figure 8(i) and were ready for polishing.

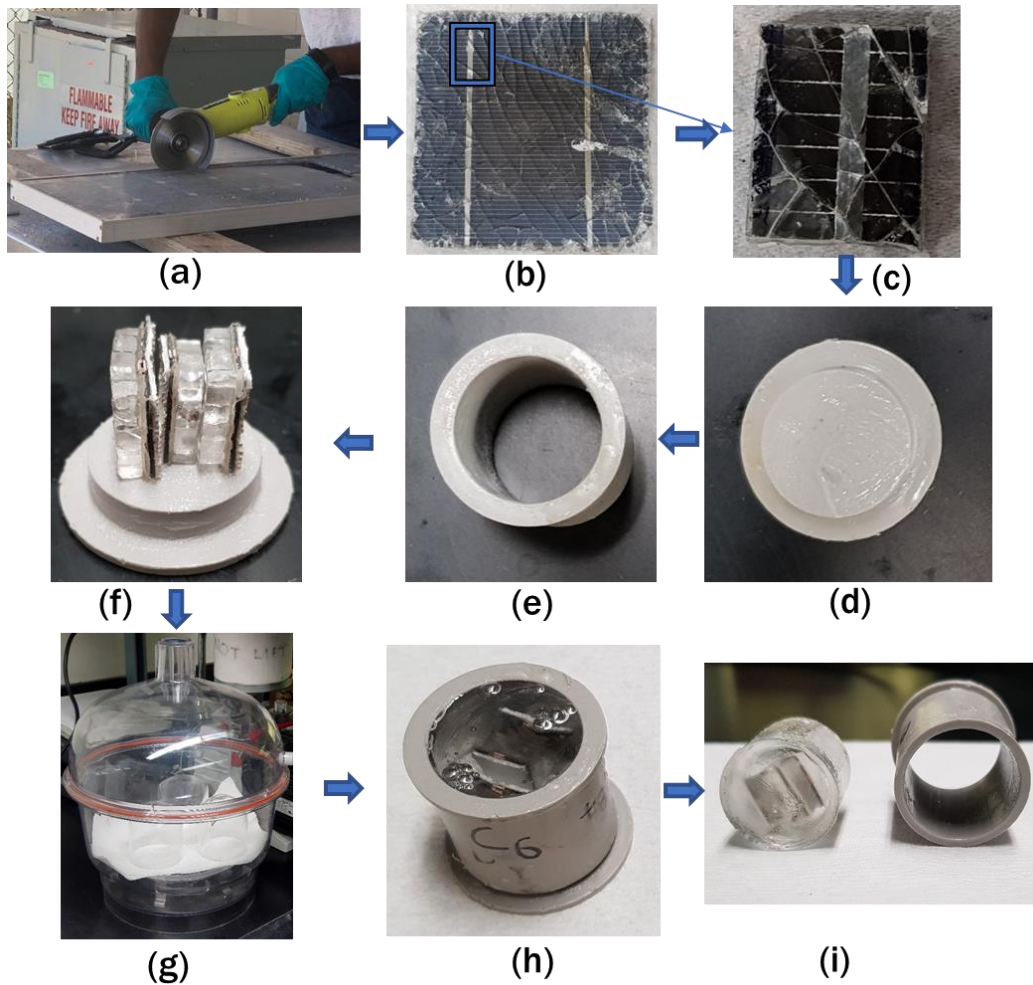


Figure 8 (a) Cutting solar cell from the module using power tool (b) Solar cell cut from the module (c) Sample cut along the interconnect region of the cell (d) Holder base coated with high vacuum grease (e) Holder cup used to contain the epoxy mix (f) Placement of the samples with the area of interest facing the base (g) Vacuum chamber used to vacuum epoxy mix (h) Uncured epoxy mix poured into the cup with samples (i) Retrieving Cured sample post 24 hours.

Post recovering the capsules are polished with 4 grades (120,240,320,600) of silicon carbide grinding paper on a grinding disc which rotates at 150 RPM. There is continuous water supply while this happens to avoid excessive heating of the samples as in Figure 9(a). The polishing is then followed by 2 grades (6 and 1 micron) of diamond grit paper rotating at 300 RPM which has a water-based lubricant as in Figure 9(b). After each grit the sample is submerged in joy and water

assembly and then placed in ultra-sonic for 30-60 sec. After polishing with each of these grits the samples are looked under optical microscope for scratches and once the scratches corresponding to each of these grits fade, the sample can be polished with the next grinding paper. Once all the scratches are polished optical microscope as in the Figure 10 is used to take optical images.



(a)

(b)

Figure 9 (a) Silicon carbide grinding paper with continuous water supply (b) Polishing cured sample to get a smooth surface for SEM and EDS analysis

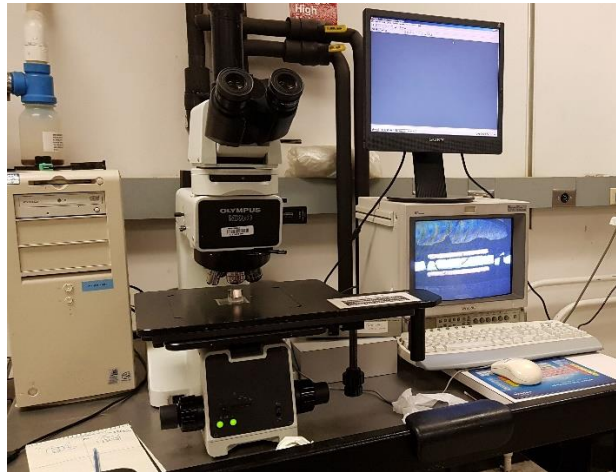


Figure 10 Optical microscope setup

The samples are then carbon coated using carbon coater as in Figure 11. A sharpened carbon rod is initially inserted in to a holder such that the sharp side rests on the flat side of the other carbon rod with enough resistance on it. The coater is then set to single pulse, 3000 ms evaporation time. The chamber is then vacuum pumped. This forms an electrically conductive layer over the top which can take away all the electrons from the surface.



Figure 11 Carbon coating setup used to coat samples with thin carbon layer

The samples post sample preparation are mounted over a metallic holder using a carbon tape which forms an electrical contact between the sample head and the bottom holder for the electrons to dissipate. The samples are then put inside the holder and calibrated as in Figure 12. the sample image is then taken using the camera at the top which can later be used to navigate the samples while the electron gun is operating. The samples are then put in vacuum inside the SEM using a vacuum pump. Once the vacuum is built the electron gun is started by applying 15 kV of voltage.

This is then followed by taking scattered electron images of the whole interconnect region at different magnifications and regions.



Figure 12 Sample placed inside the SEM holder post calibration.

3.8 EDS analysis

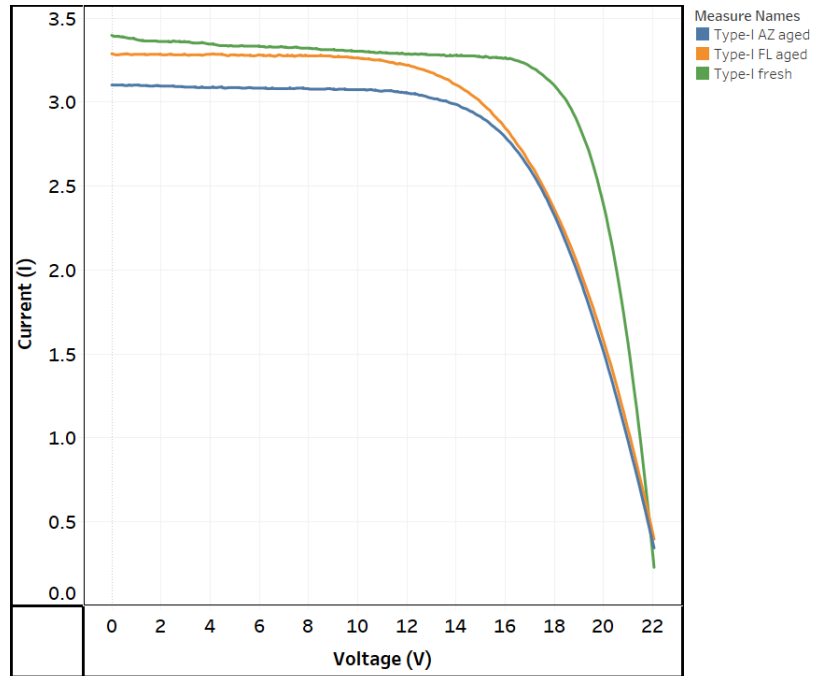
EDS will help detect the elemental composition of the sample. Line scan on EDS will help understand the extent to which there is elemental mixing and help quantify IMC thickness. The samples post SEM imaging are used for elemental analysis. Elemental maps and line scans are produced on all the images to look for intermetallic compound formation and detachment of the interconnects from the cell contacts.

4. Experimental Results

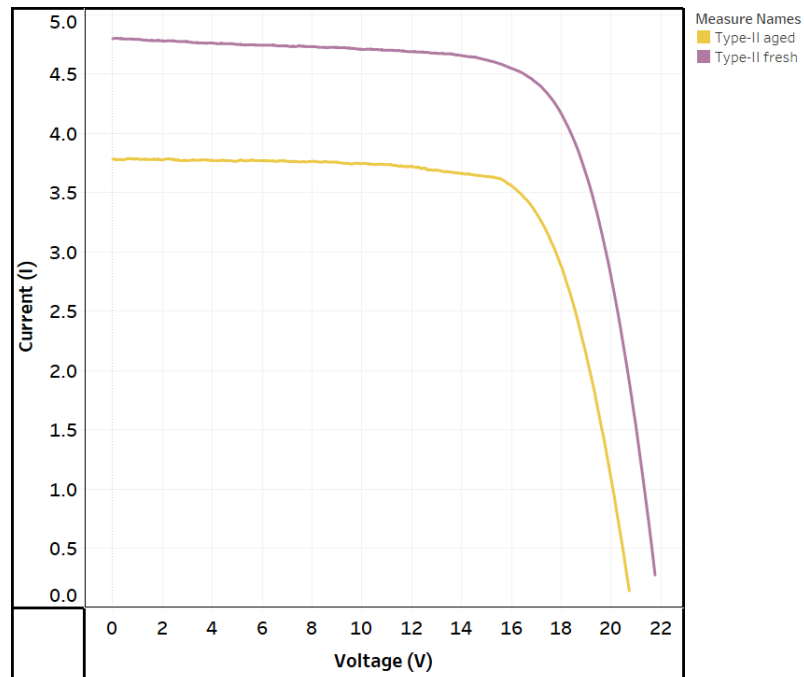
4.1 Module level performance evaluation

All the modules went through non-destructive and destructive testing to investigate the effects of ageing and climatic conditions on the solder bond degradation and its correlation with the PV performance loss. The module level IV parameters of fresh and field aged modules as in Table 2 shows that the nameplate rated and measured readings indicating the degradation over time in these modules. The IV curves of field aged modules show higher slope near V_{oc} compared to the fresh modules as in Figure 13(a) and Figure 13(b) indicating higher series resistance due to solder bond degradation and finger contact resistance increase. It also signifies that the performance losses and increase in series resistance incurred due to solder bond degradation and other degradation modes.

The module degradation rate has been calculated with respect to the name plate reading. The degradation rate for the modules can be seen in Figure 14. Type-I FL aged modules shows highest P_{max} and FF degradation where as type-I AZ aged modules shows highest I_{sc} degradation. Higher FF degradation in case of FL aged module indicates more series resistance issues compared to AZ aged modules. This is especially true when I_{sc} loss, which also contributes to FF loss is significantly lower in case of FL aged modules. The higher I_{sc} loss in AZ module can be attributed to higher degree of visible browning of the encapsulant, which is due to higher operating temperatures and ultra violet (UV) dosage in Arizona.



(a)



(b)

Figure 13 (a) IV curves of fresh and field aged type-I modules (b) IV curves of fresh and field aged type-II modules

Table 2 IV performance parameters of fresh and field aged modules

Module Name	I _{sc} (A)		V _{oc} (V)		P _{max} (W)		FF (%)	
	Rated	Measured	Rated	Measured	Rated	Measured	Rated	Measured
Type-I fresh	3.4	3.34	21.7	21.6	55	51.8	74.54	71.9
Type-I FL aged	3.4	3.25	21.7	21.5	55	40.3	74.54	57.4
Type-I AZ aged	3.35	3.101	21.7	21.5	53	43.4	72.90	63.8
Type-II fresh		4.798		21.8		75.6		72.2
Type-II AZ aged	3.89	3.61	21.4	21.3	62.5	56.8	75	73.2

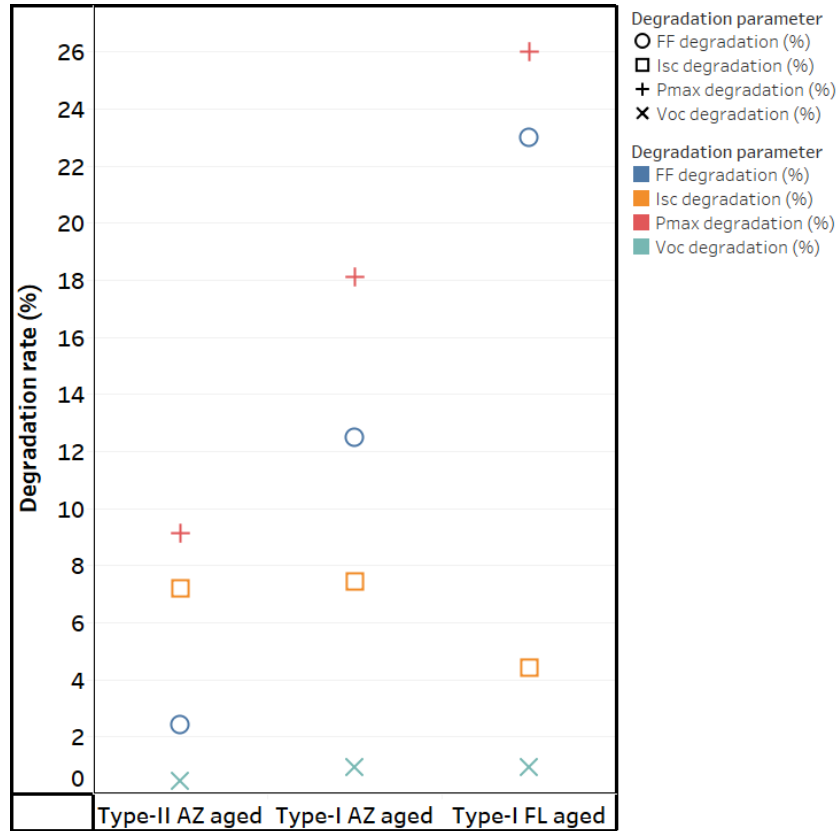
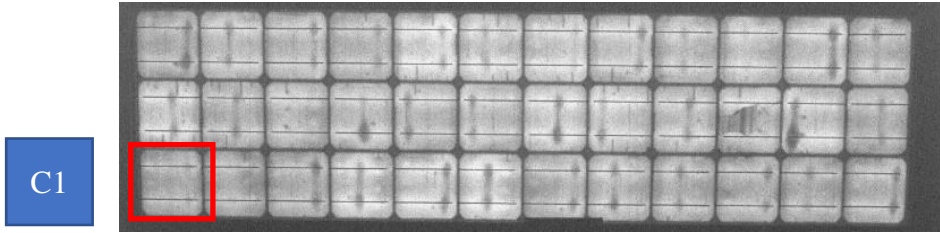


Figure 14 Plot depicting the degradation of IV parameters in test modules.

4.2 Identification of regions with degraded solder bonds

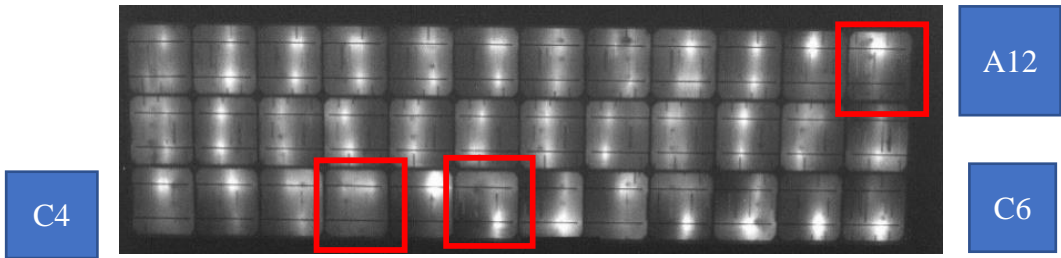
The EL images in Figure 15(a) indicate uniform luminescence in case of fresh module whereas the aged module in Figure 15(b)(c)(e) show non-uniform bright and dark regions. The dark regions here indicate electrical contact loss and the bright regions are the only paths with good electrical contact left for the current to conduct. Comparing the EL images as in Figure 15 shows the individual cells with defects and cracks in both aged and fresh modules will help pinpoint most degraded cells that accounts to the performance loses in the module. Due to interconnect detachment the cross-sectional area available for the electrons to pass through the interconnect

reduce, resulting in small pockets of bright spots as in figure available for the electrons to pass through resulting in those highly luminous spots.



C1

(a)

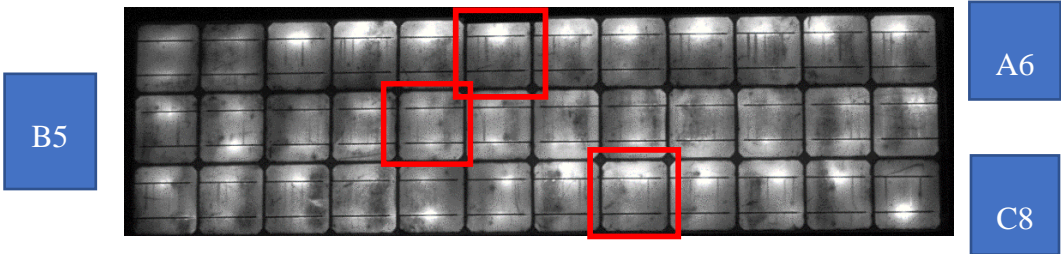


C4

A12

C6

(b)

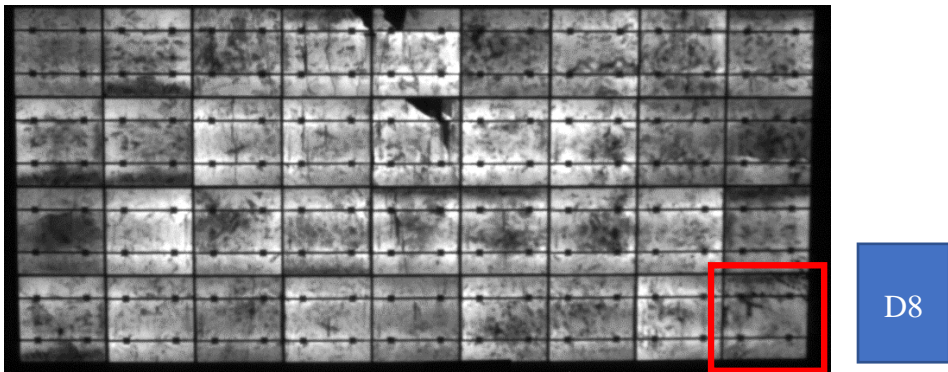


B5

A6

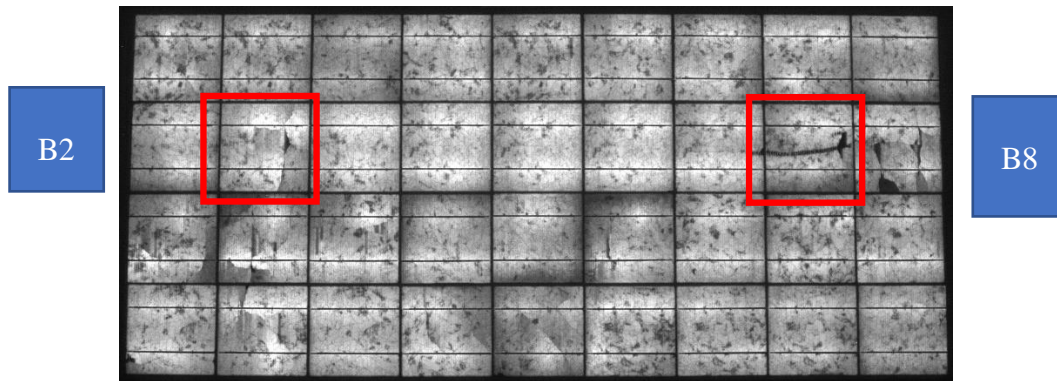
C8

(c)



D8

(d)



(e)

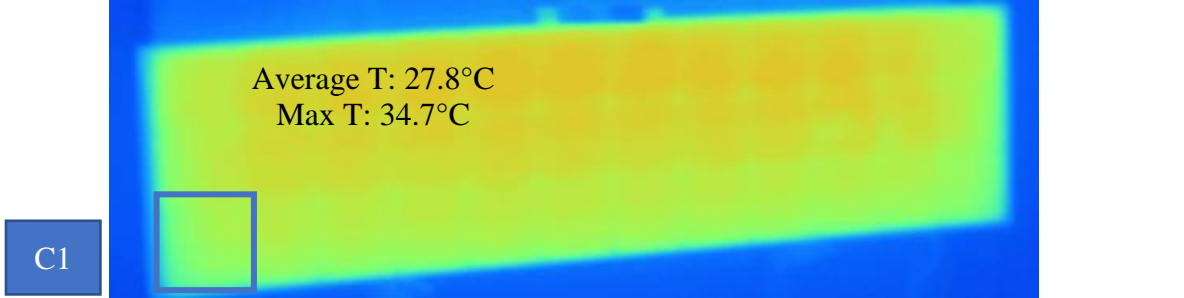
Figure 15 EL images of type-I fresh module, type-II FL aged module, type-II AZ aged module, type-II fresh module and type-II AZ aged modules in the following order.

Based on the EL images, cells with high, medium and low luminous regions were considered to be cells with high, medium and low solder bond degradation respectively. In Florida aged module cell A6, C6, C4 are selected by considering them high, medium and low degraded cells. Similarly, in Arizona aged type -I module, cells C8, A6, B5 and type -II modules cells B2 and B8 were chosen based on high, medium and low resistance cells respectively.

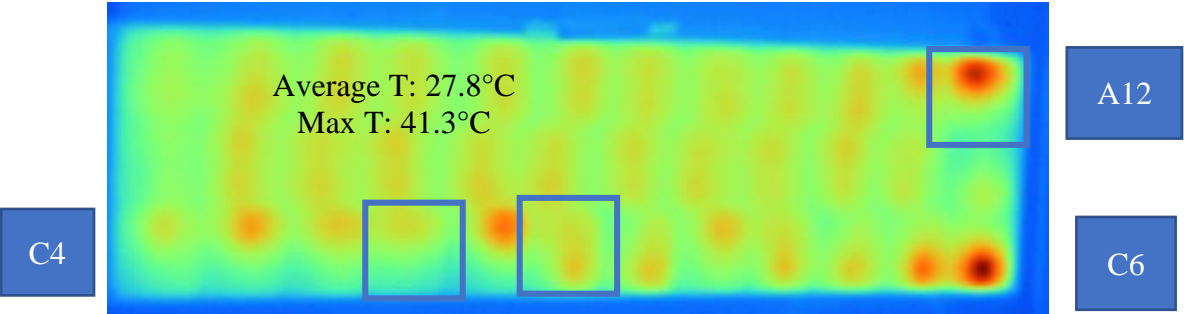
4.3 Imaging of degraded solder interconnects

The IR images show regions with higher temperatures compared to the average module temperature. These regions have higher operating temperatures in the field due to higher current density at these interconnect interfaces. The higher operating temperature as in Figure 14 further results in higher IMC formation and interconnect detachment due to reaction kinetics and CTE

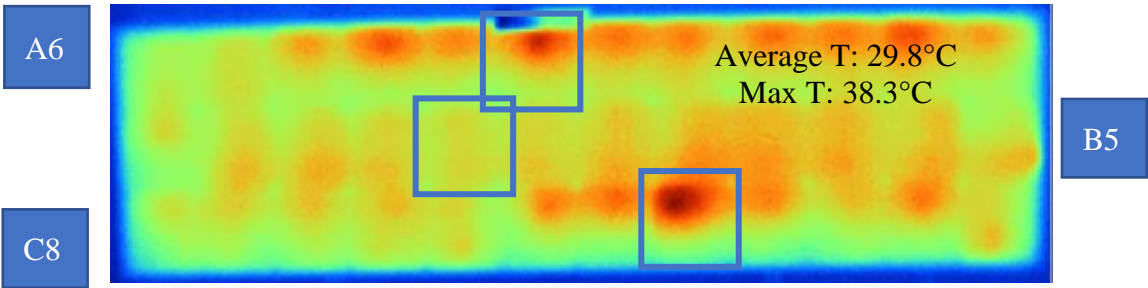
mismatch. These hot regions match with the bright spots from EL images, consolidating our initial understanding of solder bond degradation occurring due to higher current density at these regions.



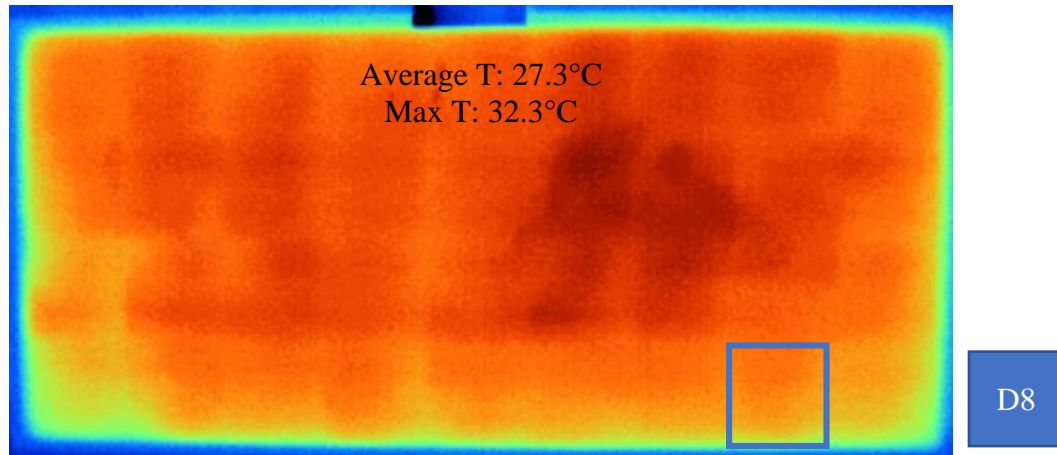
(a)



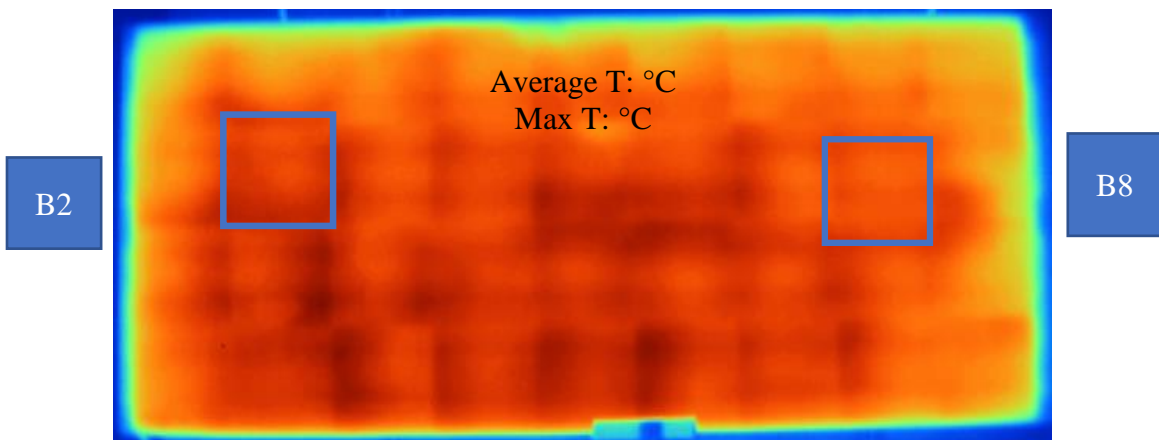
(b)



(c)



(d)



(e)



Low Temperature

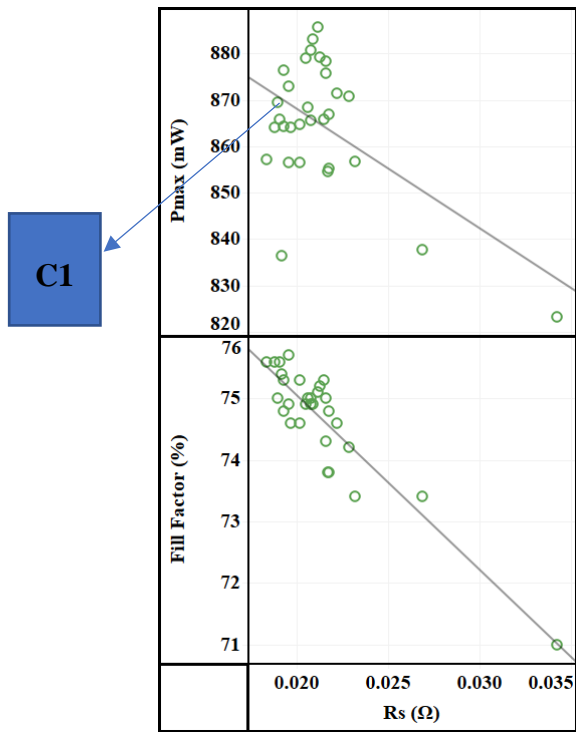
High Temperature

Figure 16 IR images of type-I fresh module, type-II FL aged module, type-II AZ aged module, type-II fresh module and type-II AZ aged modules in the following order with red being the hottest and blue being the coldest regions.

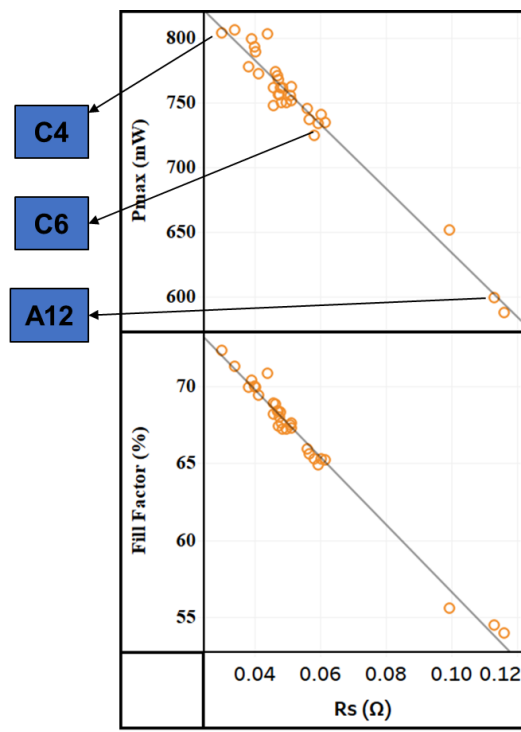
4.4 Measurement of Cell level IV parameters

The modules having all their cells backsheets cut and soldered are then measured for cell level IV parameters. Light IV and dark IV measurements were used to extract the series resistance (R_s) values from these cells. The R_s values are used to correlate with fill factor, P_{max} , bright spots on EL and hotspots on IR images.

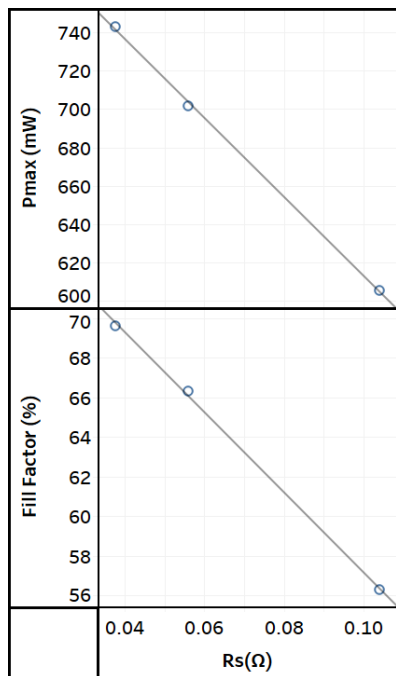
The cell level dark R_s values were plotted with respect to the cell fill factor (FF) and P_{max} values as in the image to find out the correlation coefficient. As in Figure 17(a) For type-1 FL aged modules, coefficient of determination of P_{max} and FF with R_s is 95.99% and 98.30% respectively which indicates the model to be a good fit for the data. In Figure 17(b) for type-1 fresh module the coefficient of determination of P_{max} and FF with R_s is 30% and 82.3% as the module is not degraded resulting in most of the cells being clustered around a uniform R_s value. Similarly, the correlation plots for type-II aged and field aged modules are shown in Figure 17(d) and Figure 17(e). This correlation helps better understand the effect of series resistance on the two performance parameters (R_s and FF). Based on these values the cells with low, medium and high series resistance were then selected in type-1 aged module but only one cell with least R_s is selected from type-1 fresh module.



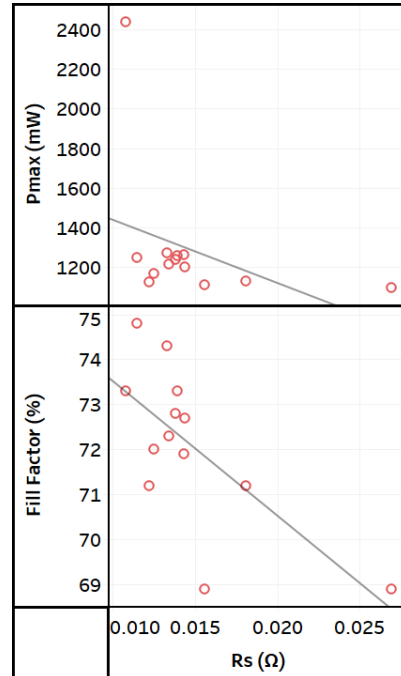
(a)



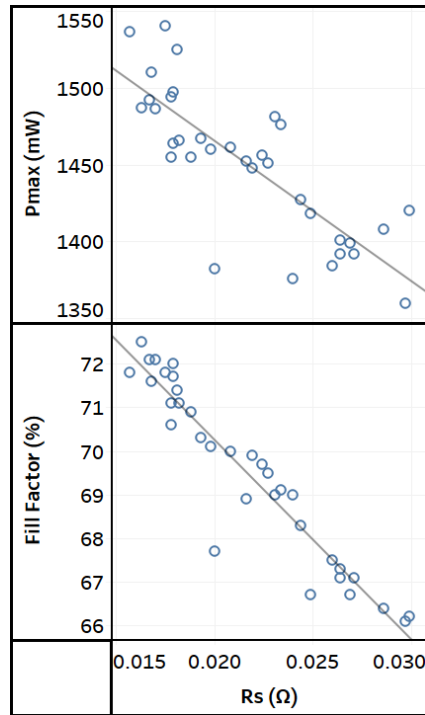
(b)



(c)



(d)



(e)

Figure 17. Maximum power (P_{max}) and Fill Factor (FF) correlation plots with series resistance (R_s) of (a) type-I fresh module (b) type-II FL aged module (c) type-II AZ aged module (d) type-II fresh module (e) type-II AZ aged modules

4.5 High resolution microscopy and elemental analysis

After sample preparation SEM images of the interconnect region were taken as in the Figure 18 (a),(b), (c). The high-resolution SEM images would be used to correlate the series resistance with the presence of intermetallic compounds and the void formation leading to detachment of the cell interconnect.

The fresh samples as in figure showed that there is very good contact between the interconnect and the busbar. This good contact also explains the low series resistance of the fresh cells.

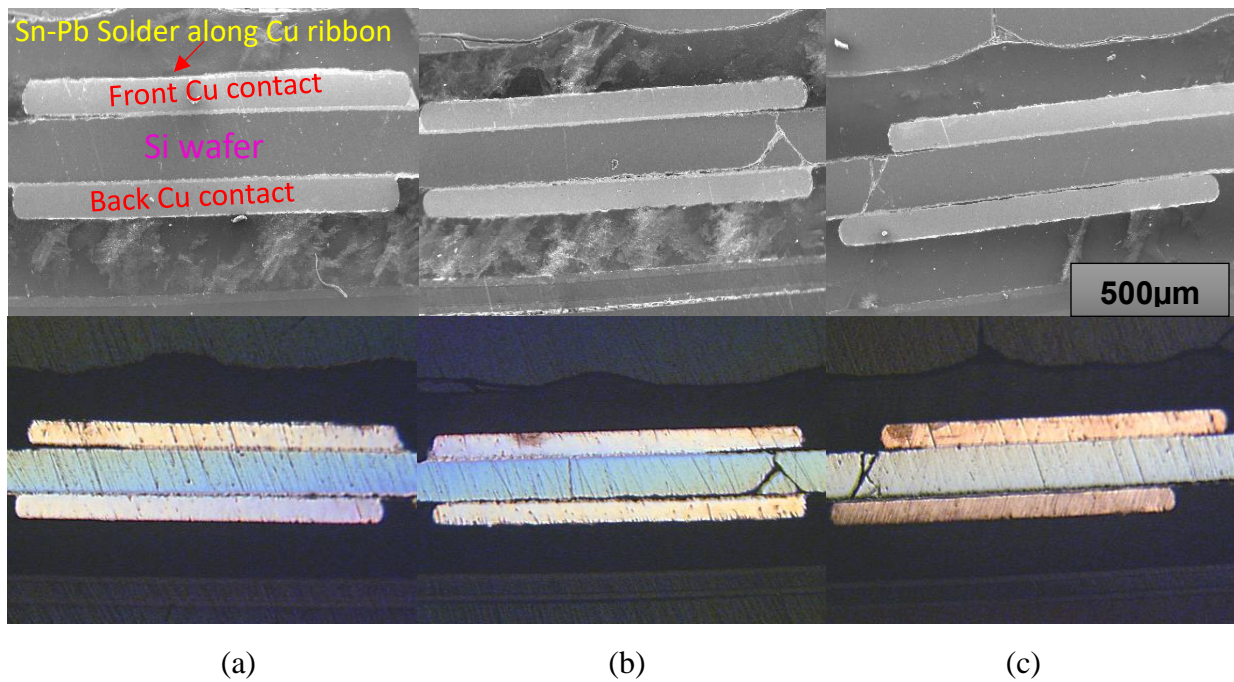


Figure 18 Cross-sectional SEM (top) and optical images (bottom) at 71X magnification of type-I fresh module with good interconnect along the back and front contacts of the cell

These good contacts from the SEM and optical images can further be confirmed by looking at the line scans results and elemental mapping results. The Figure 19 also shows the spectral measurements which indicate the elements that are present in the region. The line scan in figure indicates very less intermixing of metallic compounds. It has been shown that during the pre-tinning and the soldering process, the copper core and respectively the busbar metallization is partially dissolved into the molten solder. The high concentration of Cu and Ag atoms in the liquid solder at the interface leads to the formation of intermetallic compounds according to the phase diagrams of the respective alloy systems [11], [22]–[24]. The IMC thickness can be calculated

from the line scan graphs of top and bottom contacts as in Figure 20. The overlap of elemental compositions at the interfaces is a normal distribution curve. IMC thickness is calculated using the full width half maximum (FWHM) technique, where the overlapping bell curve between the two elements of interests are identified and the width is calculated at half the maximum height of the bell curve. The X-axis in the line scan graph is a 100-point scale and the length corresponding to these 100 points depending upon the magnification. The full width half maximum length in terms of points can then be converted to actual length. The average Ag_xSn_y thickness in fresh samples is $2.514\mu m$ and Cu_xSn_y IMC IMC is $1.626\mu m$ for both front and back contacts.

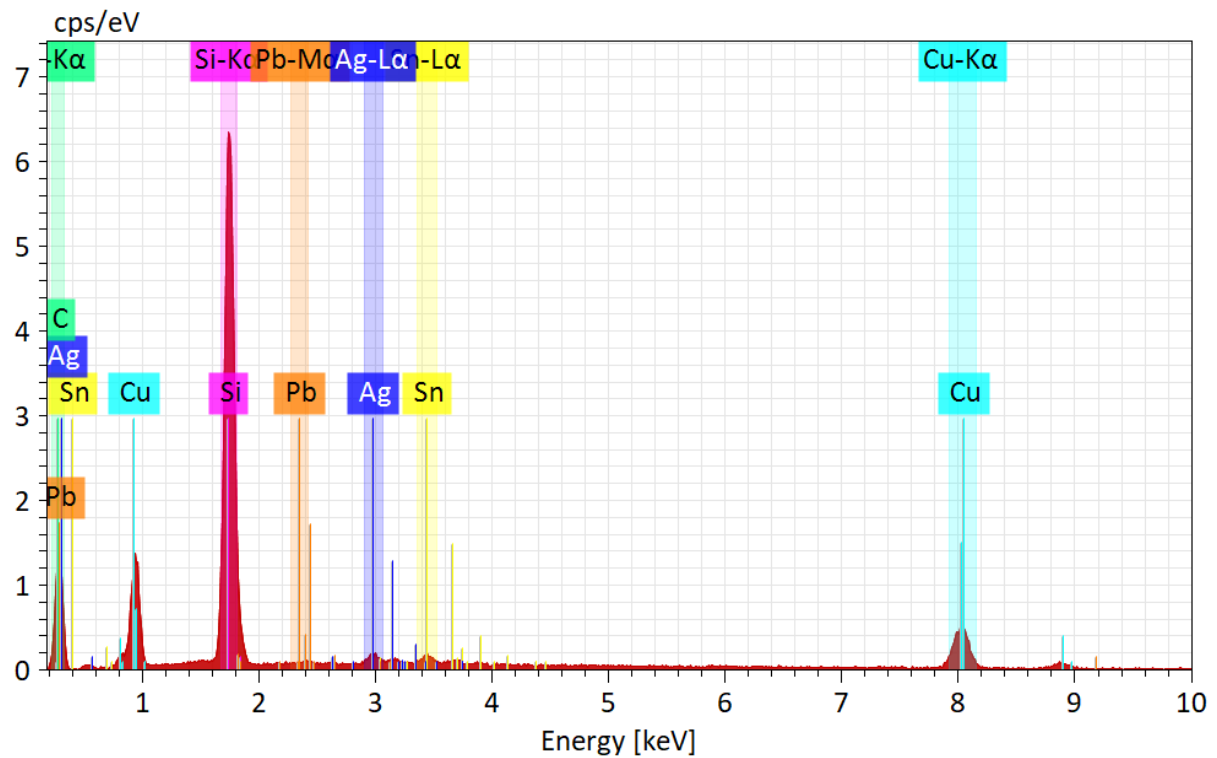


Figure 19 Elemental spectral map highlighting all the elements that are present along the interconnect region.

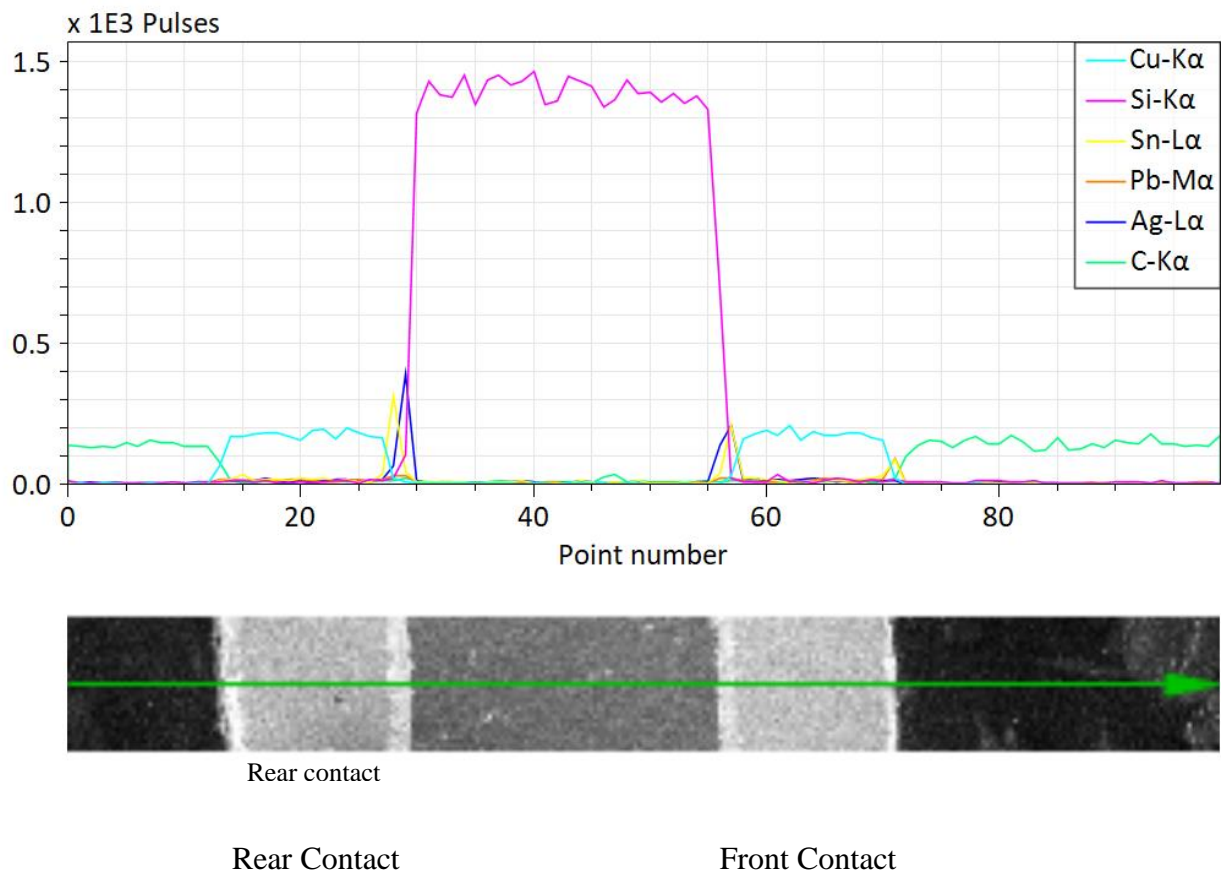


Figure 20 Line scan across the interconnect region indicating the intermixing of the adjacent metallic layers.

Figure 21 (a), (b), (c) is from Florida aged high resistance cell, it clearly indicates presence of multiple voids at the solder ribbon - Ag busbar interface at top and rear contacts. They formed due to the formation of IMC followed by detachment during thermo-mechanical fatigue. It can be observed that the rear contacts show significantly higher rates of detachment and IMC formation compared to the top contact. As suggested by [21] combination of temperature and humidity leads to higher voids formation compared to isothermal heating this could be a potential reason for this phenomenon as FL climate is humid in nature and typically there is moisture ingress from the

backsheet. The line scan in the Figure 22 indicates the formation of significant intermetallic compounds with 7.31 μm thick Ag_xSn_y and 2.54 μm thick Cu_xSn_y IMC for top contacts. The bottom contact has thicker layers with Ag_xSn_y and Cu_xSn_y IMC being 10.39 μm and 3.231 μm respectively. This further consolidates of initial hypothesis about solder bond degradation i.e. intermetallic compound formation and contact loss during thermo mechanical fatigue leads to increase in series resistance, as the cell that these samples came from has high series resistance.

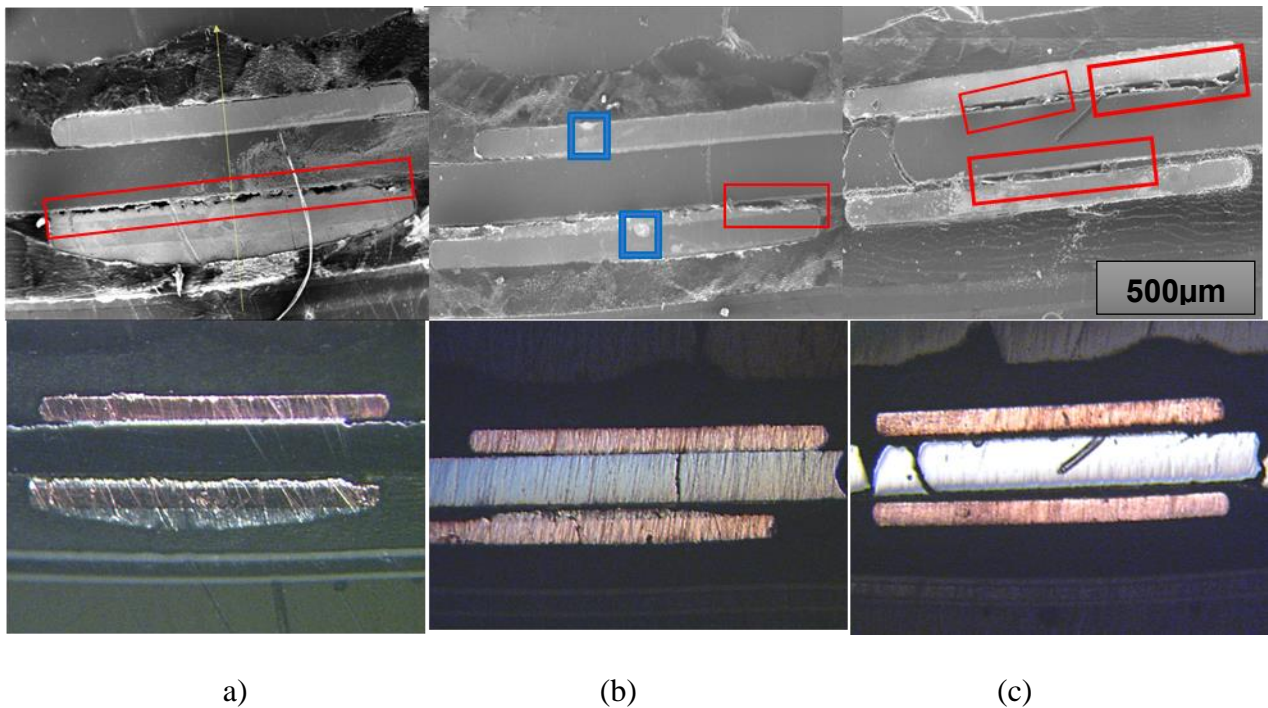


Figure 21 Cross-sectional SEM and optical images of type-I FL aged high resistance cell indicating detachment of interconnects (red box) and lead segregation (blue box)

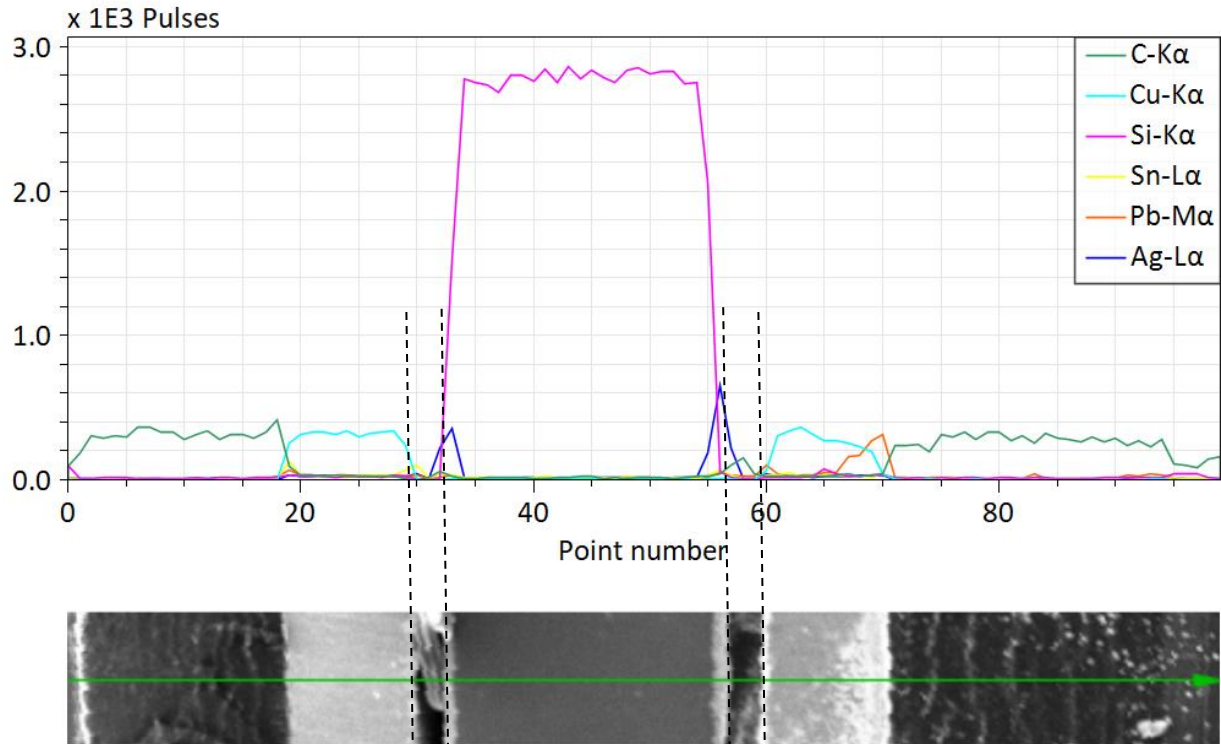
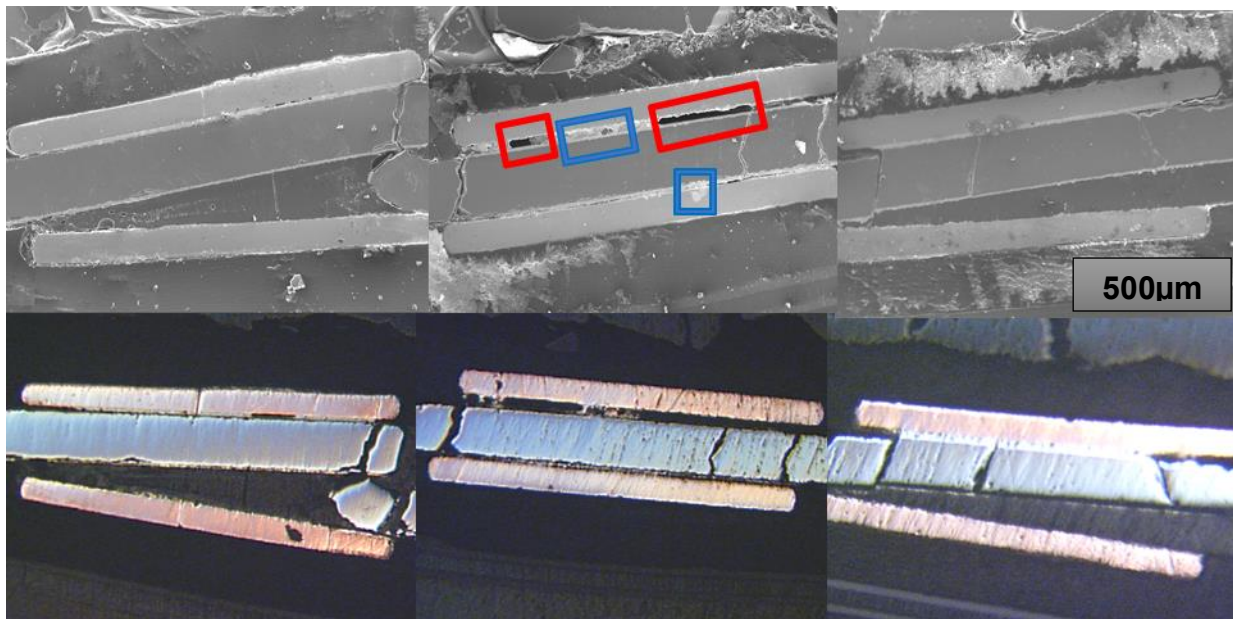


Figure 22 Line scan across the interconnect region of type-I FL aged sample-2, indicating voids at the cell-contact interface (highlighted by dotted lines).

The samples from the same module with medium Rs can be seen in Figure 23. these samples indicate comparatively lower IMC formation with 2.57 μm thick Cu_xSn_y IMC and 6.055 μm thick Ag_xSn_y for bottom contact and 4.29 μm thick Ag_xSn_y and 2.35 μm Cu_xSn_y IMC which leads to lower void formation too. The Figure 23(a), (b) has the bottom contacts that's completely detached, this detachment is not due to the mechanism that's already showed as there is no significant IMC formation at these contacts indicating detachment at this interface during manufacturing of the cell itself. EVA penetration at these interfaces further consolidate this assumption.



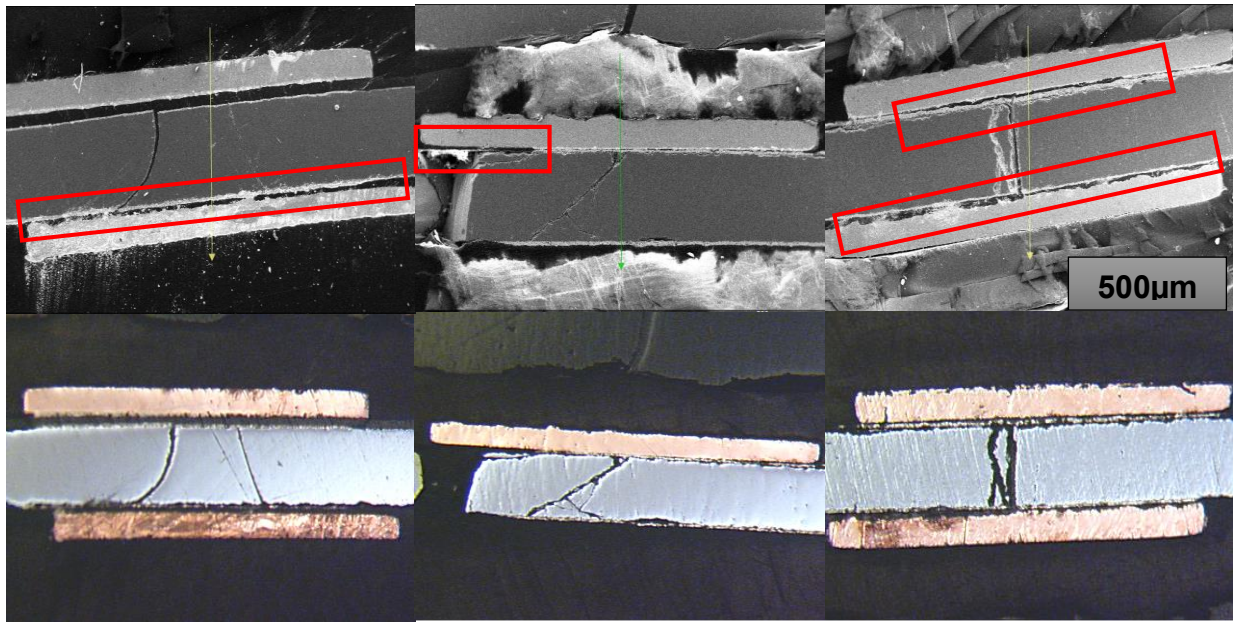
(a)

(b)

(c)

Figure 23 Cross-sectional SEM and optical images of type-I FL aged medium resistance cell samples indicating comparatively low detachment of the interconnects.

The low series resistance cell from the same module has the images as in Figure 24 . This clearly doesn't show any sign of lead segregation or detachment which is expected as the EL and IR images too doesn't show any sign of brig spots or hotspots.



(a)

(b)

(c)

Figure 25 Cross-sectional SEM and optical images of type-I AZ aged high resistance cell indicating severe detachment of interconnects (highlighted in red).

Similar trends of lower IMC formation and detachment can be seen in Figure 26 and Figure 27 as the series resistance decreases in type-1 AZ aged modules.

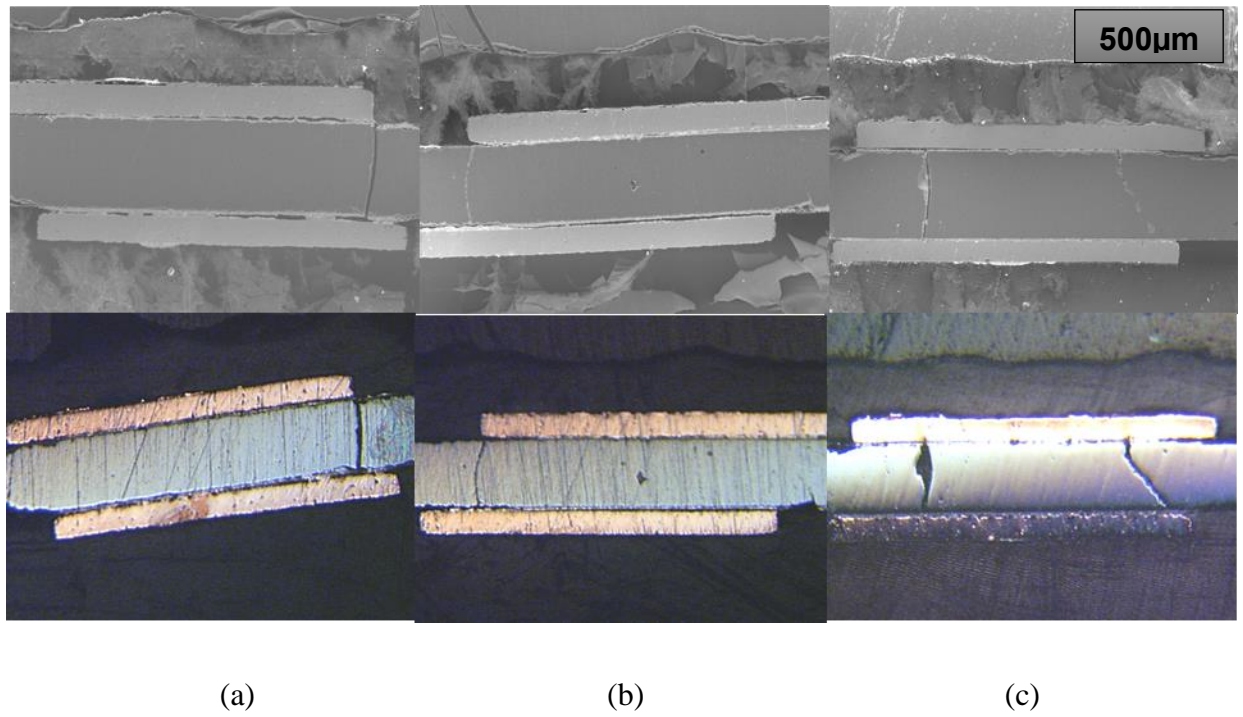


Figure 26 Cross-sectional SEM and optical images of type-I AZ aged medium resistance cell indicating comparatively low detachment

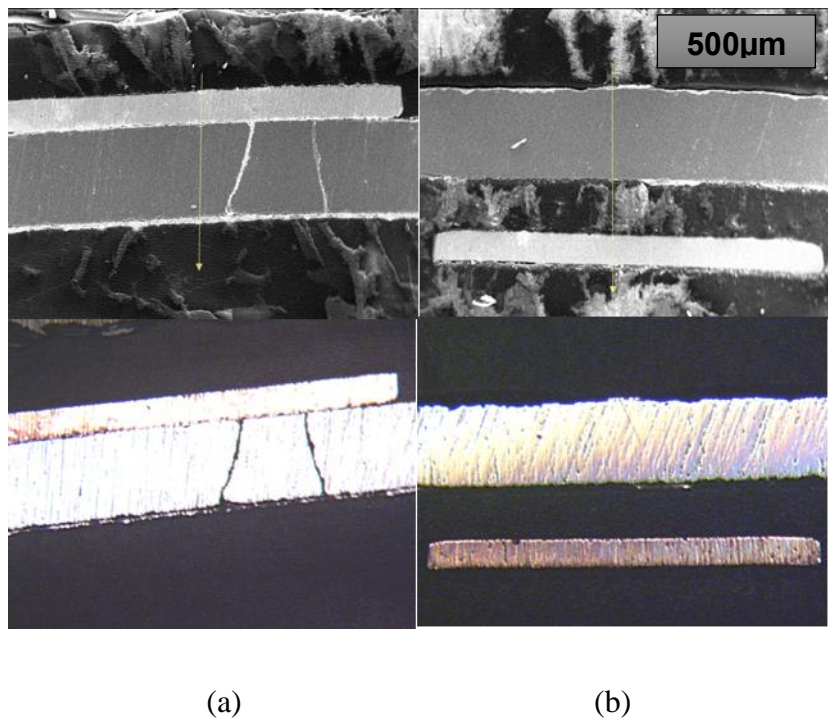


Figure 27 Cross-sectional SEM and optical images of type-I AZ aged low resistance cell indicating low detachment of interconnects.

The type-2 fresh module has a different solder composition with Ag being an additional component but due to the low sensitivity of the SEM instrument the 3 wt% of Ag could not be detected in the EDS analysis. The Figure 28 shows the contacts to be slightly detached from the busbar. The possible reason for this could be due to the breakage of solar cell during sample preparation the type-2 module having a multi-crystalline solar cell is more susceptible to cracking. The detachment here can be said not due to the previous mechanism of IMC formation and thermo-mechanical fatigue as the line scan in the Figure 29 clearly indicates discrete elemental regions.

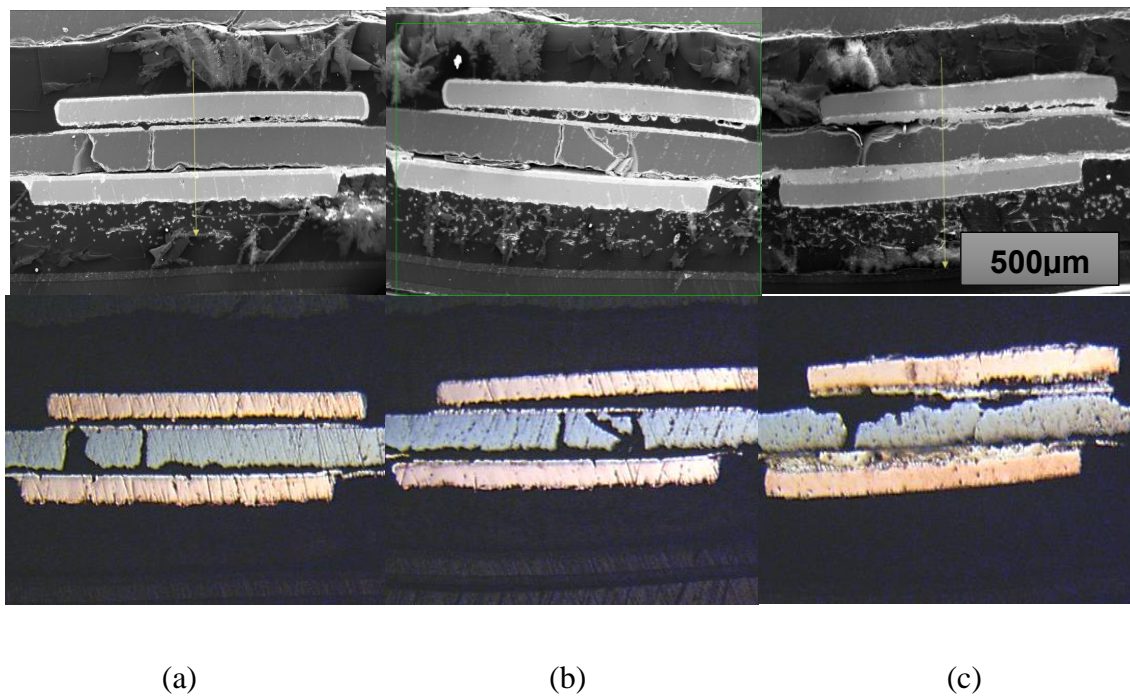
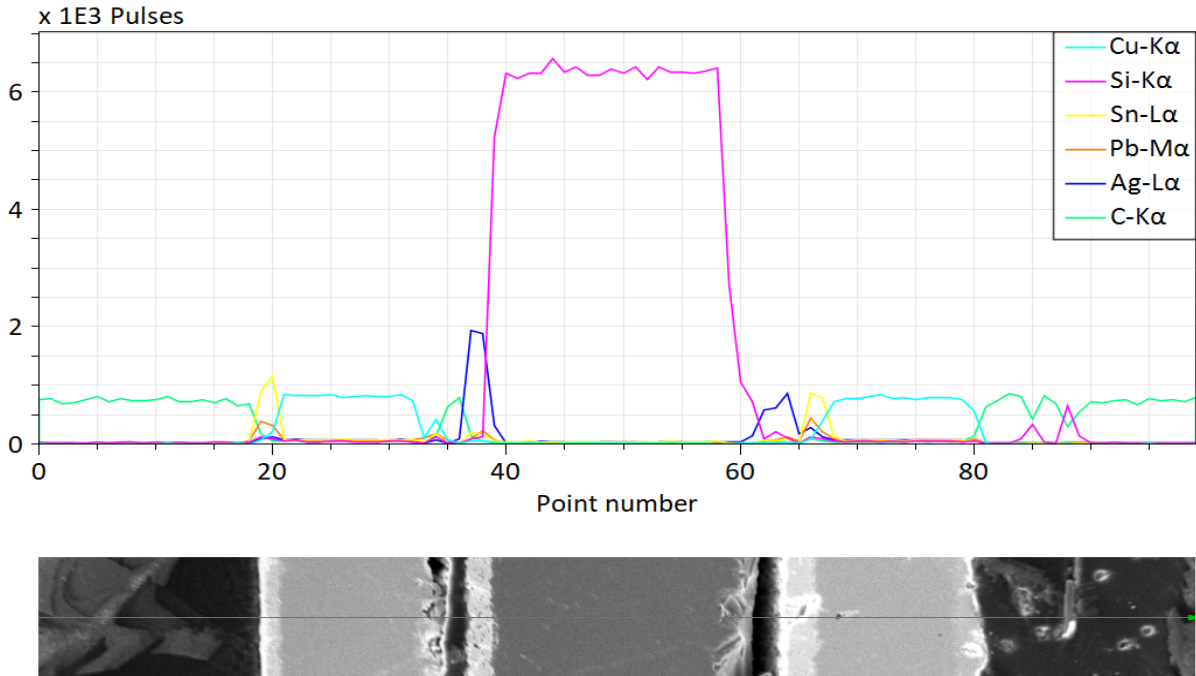


Figure 28 Cross-sectional SEM and optical images of type-II fresh module.



Name	Date	Time	Points	Length [mm]
BSE Compare	9/26/2018	2:56:24 PM	100	992.9 μm

Figure 29 Line scan across the interconnect region of type-II AZ aged sample-1

Type-II aged samples as in Figure 30 have IMC formation followed by detachment as IMC thickness and detachment can be verified from elemental overlap and encapsulant penetration along the Sn and Ag interfacial layers from the linescan. The layers can be identified from the line scan as in Figure 31, due to overlapping elemental lines it is difficult to quantify the thickness as the layers are already detached and the IMC layers are fractured. This samples due to weak interfacial layers also shows higher amounts of detachment leading to EVA penetration into these spaces. This phenomenon of detachment and EVA penetration can be clearly seen in the line scan. The line scan in figure clearly shows the detachment of bottom contact solder layer.

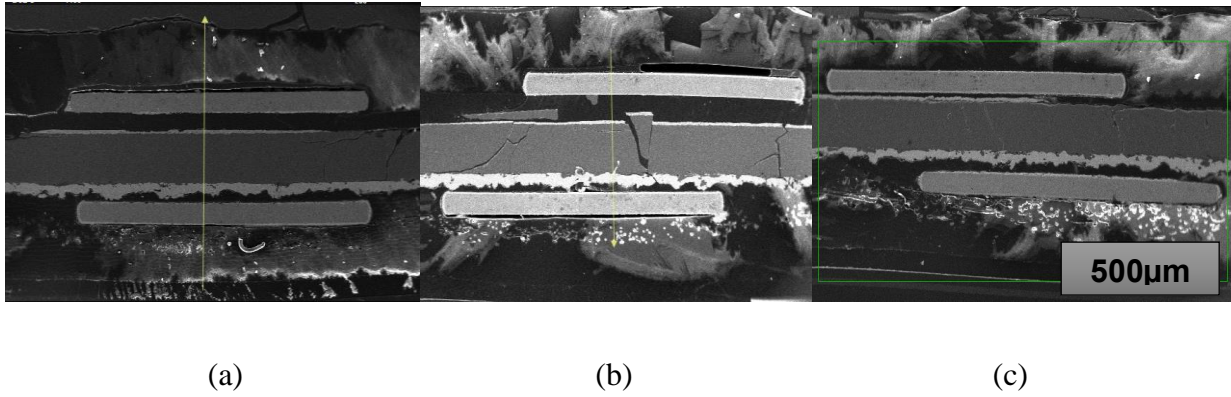


Figure 30 Cross-sectional SEM of type-II AZ aged low resistance cell indicating low detachment of interconnects.

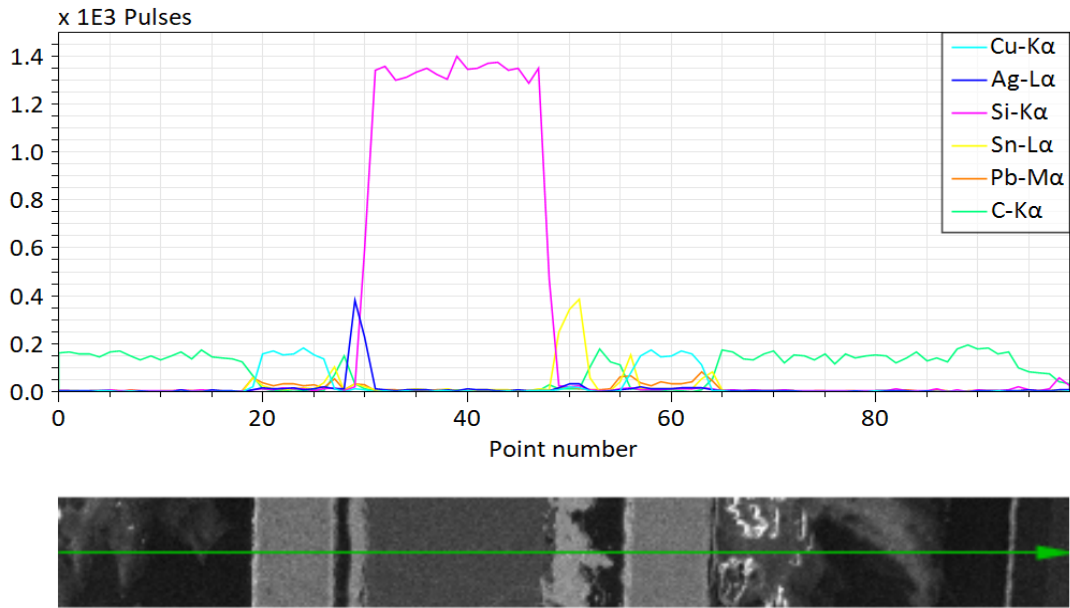


Figure 31 Line scan across the interconnect region of type-II AZ aged sample-2

The box plot in Figure 32 indicates the trends in module IMC thickness and series resistance among type-I modules from different climates. The plot clearly indicates a decreasing trend in cell level Rs with AZ field-aged being highest and fresh being the lowest. This could be understood from

the fact that Arizona module was 18-year field aged while Florida module was 10-year old along with the fact that the operating temperature are higher in AZ compared to FL.

In case of Ag_xSn_y , FL module has thicker IMC due to the role of humidity along with temperature dominating the IMC formation [21]. When it comes to Cu_xSn_y system, IMC is higher in AZ module compared to FL module since intermixing diffusivity of Cu_xSn_y system is higher than that of Ag-Sn system [25], [26]. Table 3 shows a good summary of results that correlate degraded solder bond image to their corresponding series resistance value.

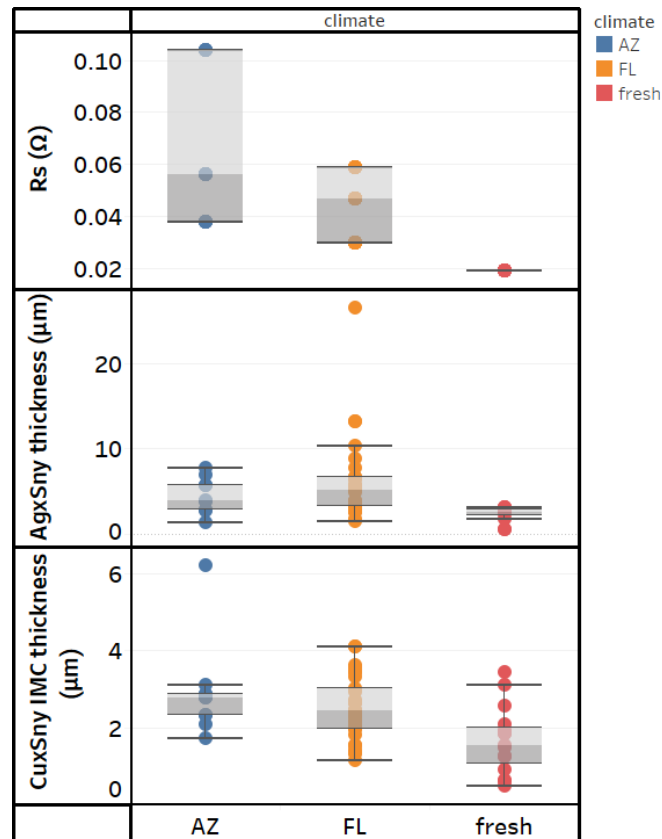
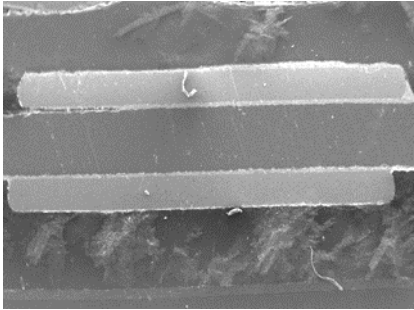
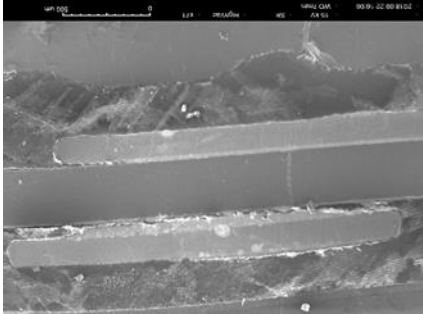
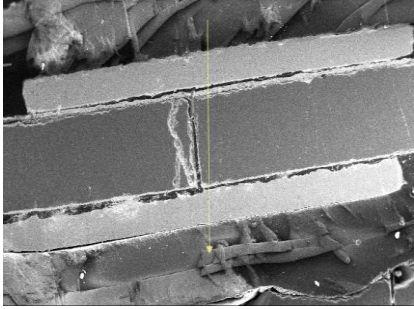
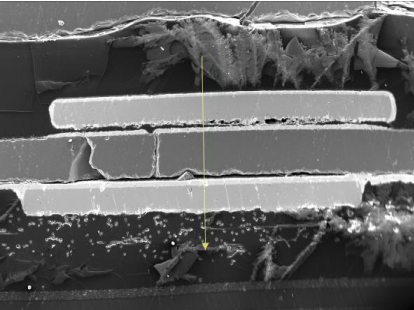
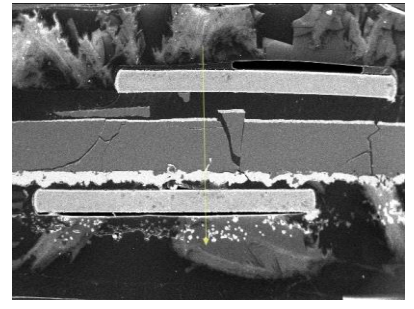


Figure 32 Series resistance and IMC thickness boxplot of aged and fresh modules.

Table 3 Summary of results showing correlation between interconnect detachment in SEM images and cell series resistance values.

Name	SEM Image	Cell Rs (Ω)	Comments
Type-1 fresh		0.019 Ω	The interconnects here have very good contact with the busbars
Type-1 FL aged (10 years)		0.059 Ω	The IMC formation and detachment at the rear contact is accelerated due to oxide formation in the presence of moisture.

<p>Type-1 AZ aged (18 years)</p>		<p>0.104 Ω</p>	<p>Being in a dry climate led to IMC formation and detachment equally on both contacts</p>
<p>Type-2 fresh</p>		<p>0.0143 Ω</p>	<p>The fresh samples have IMC from manufacturing. The detachment of interconnect is due to broken cell pieces</p>
<p>Type-2 AZ aged (xx years)</p>		<p>0.0299Ω</p>	<p>The IMC formation and detachment in this case is higher as the module is towards the end of its life.</p>

5. Conclusions

Two types of Aged and fresh modules from AZ and FL have been evaluated for quantifying the effects of solder bond degradation on series resistance increase and to identify the mechanism of intermetallic compounds formation in different locations. Solder bond degradation has been quantified based on thickness of the intermetallic compounds and detachment of the interconnects from the metal contacts. The following observations has been made

1. IMC initially forms at the interconnect and contact interface during soldering at high temperatures and it grows due to solid state diffusion in the field.
2. Combination of IMC growth and detachment of interconnects due to void formation and crack propagation has been observed.
3. Good correlation between the R_s degradation and solder bond degradation through IMC growth and void formation has been established in field aged modules.
4. Though AZ modules are 18 years old, type-I FL aged interconnects showed thicker Ag_xSn_y IMC at rear contacts due to formation of metal oxides in presence of moisture. As FL is a humid climate, the modules are more susceptible to moisture ingress through backsheet.
5. In case of Cu_xSn_y IMC, type-I AZ module has thicker Cu_xSn_y compared to type-I FL aged module. This is due to the fact that the diffusivity of Cu is three orders higher than Ag in Sn and this phenomenon dominates the metal oxide formation.
6. Although the thickness of IMC is important in determining the possibility of future detachment, it's the contact loss that results in actual increase in series resistance and performance loss. This can be seen from higher performance loss in AZ aged modules due

to contact loss at front and rear contacts when compared to FL aged modules which have only rear contact loss.

References

- [1] P. Sundarajan, “Defects and Statistical Degradation Analysis of Photovoltaic Power Plants,” 2016.
- [2] M. A. Green, “Commercial progress and challenges for photovoltaics,” *Nat. Energy*, vol. 1, no. 1, p. 15015, 2016.
- [3] A. M. D. Pysch and S. W. G. , A. Filipovic, “Detailed Analysis of Fine Printed and Plated Solar Cell Contacts,” in *22nd European Photovoltaic Solar Energy Conference and Exhibition*, 2006, no. September, pp. 3–7.
- [4] A. Tummala, *Effect of Series Resistance Increase on Fill Factor of PV Cells Extracted from Field Aged Modules of Different Climates*, no. July. 2016.
- [5] U. Itoh, M. Yoshida, H. Tokuhisa, K. Takeuchi, and Y. Takemura, “Solder joint failure modes in the conventional crystalline si module,” *Energy Procedia*, vol. 55, no. 3, pp. 464–468, 2014.
- [6] T. Geipel, M. Moeller, A. Kraft, and U. Eitner, “A Comprehensive Study of Intermetallic Compounds in Solar Cell Interconnections and their Growth Kinetics,” *Energy Procedia*, vol. 98, pp. 86–97, 2016.
- [7] B. Simeková and K. Ulrich, “Kinetics of intermetallic phase formation at the interface of Sn – Ag – Cu – X (X = Bi , In) solders with Cu substrate,” vol. 509, pp. 7052–7059, 2011.
- [8] Y. W. A. S. P. A. F. L. M. G. J. F. Pinizzotto, “The formation and growth of intermetallics in composite solder,” *J. Electron. Mater.*, vol. 22, no. 7, pp. 769–777, 1993.
- [9] J. O. G. P. D. L. C. M. Bernstein, “Effects of intermetallic formation at the interface between copper and lead-tin solder,” *J. Mater. Sci.*, vol. 23, no. 7, pp. 2564–2572, 1988.
- [10] D. R. F. T. Vianco, “Intermetallic growth and mechanical behavior of low and high melting temperature solder alloys,” *Metall. Mater. Trans. A*, vol. 25, no. 7, pp. 1509–1523, 1994.
- [11] A. C. K. So, Y. C. Chan, S. Member, and J. K. L. Lai, “Aging Studies of Cu – Sn Intermetallic Compounds in Annealed Surface Mount Solder Joints,” vol. 20, no. 2, pp. 161–166, 1997.

- [12] P. L. Tu, Y. C. Chan, S. Member, and J. K. L. Lai, "Effect of Intermetallic Compounds on the Thermal Fatigue of Surface Mount Solder Joints," vol. 20, no. 1, pp. 87–93, 1997.
- [13] K. Zeng and K. N. Tu, "Six cases of reliability study of Pb-free solder joints in electronic packaging technology," vol. 38, pp. 55–105, 2002.
- [14] K. Morita, T. Inoue, H. Kato, I. Tsuda, and E. T. Laboratories, "Degradation Factor Analysis of Crystalline-Si PV Modules Through Long-Term Field Exposure Test," pp. 1948–1951, 2003.
- [15] E. E. Van Dyk, J. B. Chamel, and A. R. Gxasheka, "Investigation of delamination in an edge-defined film-fed growth photovoltaic module," vol. 88, pp. 403–411, 2005.
- [16] N. G. Dhere and N. R. Raravikar, "Adhesional shear strength and surface analysis of a PV module deployed in harsh coastal climate," vol. 67, pp. 363–367, 2001.
- [17] X. Han, Y. Wang, L. Zhu, H. Xiang, and H. Zhang, "Mechanism study of the electrical performance change of silicon concentrator solar cells immersed in de-ionized water," *Energy Convers. Manag.*, vol. 53, no. 1, pp. 1–10, 2012.
- [18] D. Polverini, M. Field, E. Dunlop, and W. Zaaiman, "Polycrystalline silicon PV modules performance and degradation over 20 years," no. April 2012, pp. 1004–1015, 2013.
- [19] V. Jung and U. Eitner, "Requirements on Metallization Schemes on Solar Cells with Focus on Photovoltaic Modules," 2010.
- [20] C. Dechthummarong, B. Wiengmoon, D. Chenvidhya, C. Jivacate, and K. Kirtikara, "Solar Energy Materials & Solar Cells Physical deterioration of encapsulation and electrical insulation properties of PV modules after long-term operation in Thailand," *Sol. Energy Mater. Sol. Cells*, vol. 94, no. 9, pp. 1437–1440, 2010.
- [21] J. Yoon, B. Noh, Y. Lee, H. Lee, and S. Jung, "Microelectronics Reliability Effects of isothermal aging and temperature – humidity treatment of substrate on joint reliability of Sn – 3 . 0Ag – 0 . 5Cu / OSP-finished Cu CSP solder joint OSP finished Cu SMD (Solder Mask Define) type," *Microelectron. Reliab.*, vol. 48, no. 11–12, pp. 1864–1874, 2008.
- [22] T. Laurila, V. Vuorinen, and J. K. Kivilahti, "Interfacial reactions between lead-free solders and common base materials," *Mater. Sci. Eng. R Reports*, vol. 49, no. 1–2, pp. 1–60, 2005.
- [23] M. A. P. Saunders N., "The Cu–Sn (copper–tin) system," *Bull. Alloy Phase Diagrams*, vol. 11, pp. 278–287, 1990.

- [24] I. K. T. Thompson, "The Ag-Sn (silver-tin) system," *Bull. Alloy Phase Diagrams*, vol. 8, no. 4, pp. 340–347, 1987.
- [25] F. Gao and J. Qu, "Calculating the diffusivity of Cu and Sn in Cu₃Sn intermetallic by molecular dynamics simulations," *Mater. Lett.*, vol. 73, pp. 92–94, 2012.
- [26] K. Suzuki, S. Kano, M. Kajihara, N. Kurokawa, and K. Sakamoto, "Reactive Diffusion between Ag and Sn at Solid State Temperatures," vol. 46, no. 5, pp. 969–973, 2005.